Dear Editor,
Thank you very much for the opportunity to improve our manuscript.
The referee's questions are in black. Our answers are in blue.

Reply to the comments of 1st Referee:

Comment1: This manuscript examined some inconsistencies with the use of the Goddard Chemistry Aerosol Radiation and Transport (GOCART) aerosol module in the fully coupled WRF-Chem model. The authors identified that 1) the diagnostic output of PM2.5 surface concentration was underestimated by 7% and PM10 surface concentration was overestimated by 5% due to the incorrect representation of the dust and sea salt coefficients; 2) the contribution of sub-micron (0.1 – 0.46 ï ¸A m) dust particles was underestimated in the calculation of optical properties with the consequence of underestimated AOD by 25-30% because the finer dust particles were not accounted for in the Mie calculations; and 3) an inconsistency in dealing with gravitational settling that led to the overestimation of the dust column loadings by 4-6%, PM10 surface concentrations by 2-4%, and the rate of gravitational settling by 5-10%. The authors further examined the impacts of boundary conditions on PM10 surface concentrations using the MERRA-2 reanalysis. These are all useful aspects of the WRF-Chem model and certainly help the improvement of the WRF-Chem simulations. However, this manuscript lacks indepth technical and scientific analyses and is rather poor scientifically. All the analyses were based on one dust case (1-12 August, 2016) over the Middle East which calls into question the applicability and effectiveness of the code rectifications in other regions and in other dust cases under different meteorological and land surface conditions. Besides, I have several major concerns as listed below:

We thank the reviewer for the valuable comments.
We disagree with the statement related to the technical and scientific merits of our study. The paper discusses the inconsistencies we found in the WRF-Chem v3.2 code released on April 2, 2010. We cooperated with the model developers to test and implement those corrections in the newly released WRF-Chem v4.1.3. The main objective of the presented paper is to quantify the effect of those inconsistencies on model performance.

Specifically, our findings explain why WRF-Chem overestimated PM10 surface concentrations, and why realistic values of AOD were associated with overly strong dust emissions and elevated dust surface concentrations. These discrepancies have been discussed in some previous studies: Kumar et al. (2014); Eltahan et al. (2018); Flaounas et al. (2017).

Our numerical experiments are specifically chosen to demonstrate the effect of those corrections quantitatively. It is not vitally important which region of the world is selected for our experiments, just that it should be a dusty region. We use a WRF-Chem experimental setup configured over the Middle East, one of the most significant dust source regions. Specific dust event cases were not considered. Different meteorological and surface conditions will not affect the results since we estimate relative biases, not absolute values.

Comment 1: The Introduction section was poorly written. It is clear that the authors have read and cited a lot of references on the subject of dust sources, dust impacts and dust modeling but the Introduction section was written in such a way that it was hard to gain a clear idea of why the inconsistencies occur and what the latest developments are in dealing with them and how the authors would like to address them. The Introduction section needs to be improved substantially.

We agree with this assessment. Accordingly we have shortened and improved the introduction section and clarified the text overall.

Comment 2: How were the “correct” dust and sea salt coefficients, d_25, s_25, d_10, in Equation 2, determined? The authors mentioned that they used the natural logarithm of particle radii but what was the rationale behind that? Was that determined from empirical relationships or lab experiments or field measurements or just trial and error? Are there any references for that?

Calculation of PM2.5 and PM10 concentrations requires the integration of aerosol volume size distribution (approximated in GOCART by five bins for dust and by three bins for sea salt) over the radius r from 0 to 2.5 um and from 0 to 10 um, respectively. Integration could be done assuming that the size distribution is a function of r or ln(r). Coefficients d_25, s_25, d_10 in eq.2 are obtained assuming that the aerosol size distribution is a function of ln(r). This method is acknowledged in CAMS reanalysis (https://confluence.ecmwf.int/pages/viewpage.action?pageId=153393481) and is justified by the fact that an aerosol size distribution is a smoother function of ln(r) than r, and therefore numerical integration is more accurate. The coefficients s_25, d_25 d_10 in the original WRF-Chem v3.2 were calculated incorrectly.

Comment 3&4: I commend the authors for identifying the underestimation of the AOD by the neglect of the sub-micron dust particles and their effects but I am concerned that the authors did not provide any logic behind the modifications of the corresponding numbers from MOZAIC bins (1, 2, 3, 4, 5, 6, 7, 8) to GOCART dust bins (DUST1, 2, 3, 4, 5). Please provide scientific evidence or references to support this work. Otherwise, what the authors have done is not convincing at all. 4) The authors changed the calculation of bin concentrations of dust and sea salt from using the functions of particle radius to using the functions of natural logarithm of radius. Again, what was the rationale behind this?

The mapping of GOCART five dustbins approximation of the aerosol size distribution to the MOSAIC eight bins also requires the interpolation of aerosol size distribution over the radius r or ln(r). Consistent with our calculation of PM2.5 and PM10, we assume that the aerosol size distribution is a function of ln(r). In the course of interpolation we conserve the integral of volume size distribution, i.e., total volume of particles. The rationale is that the size distribution is a smoother function of ln(r) than r, and therefore both interpolation and integration are more accurate in the ln(r) space. Table 4 compares the bins’ partitions calculated assuming aerosol size distribution is a function of ln(r) or r.

Comment 5: I did not understand how the inconsistency in the gravitational setting of dust and sea salt led to the increase of their total mass in the atmosphere. The authors mentioned that “Instead of transport the dust and sea salt mass between the layers, the default finite-difference scheme transport their mass mixing ratios not taking into account the dry air density variation with the height”. Does this mean that dust and sea salt mass can’t be transported across the layers? If there are vertical motions or turbulence dust and sea salt can certainly move up and down. Then where did this overestimation come from?

In the previous versions of WRF-Chem coupled with GOCART, the mass flux of gravitationally deposited material (dust and sea salt) was miscalculated. The outgoing mass flux from the bottom of each grid cell was overestimated. As a result, the integral mass balance was violated. In the paper we present a conservative finite difference scheme that correctly

approximates gravitational deposition. We conducted a numerical experiment which shows that the old scheme violates the mass balance, whereasthe new one does not.

6) The English of this manuscript needs to be improved.

Thank you for your comment, with which we agree. We have now thoroughly re-edited and improved the text of the manuscript for clarity of meaning and readability.

Minor concerns:

1) On Line 21-22 of Page 8 the authors stated that "The model erroneously pushed more dust into the atmosphere to fit the observed AOD". Was this in reference to the model default values or the model runs that assimilate the observed AOD. I don't quite understand this.

Here we compare two runs with and without corrections. The model without corrections underestimates the AOD. Therefore in order to reproduce observed AOD, more dust is required to be emitted. Because AOD was underestimated, we conclude that this increased dust emission is also erroneous, and treat it as overestimation of dust emission. This is in line with the cases discussed in the literature, when dust emission is tuned to reproduce AOD and it overestimates PM surface concentrations. The text has corrected to clarify this issue.

2) I did not understand this statement on Line 16-18 of Page 10: "In both runs, the magnitude and temporal evolution of the AOD time-series are well correlated with the observed AERONET AOD at all sites only in the absence of dust events or when the AERONET AOD is below 1". I am wondering what the authors wanted to convey here with this statement.

We wanted to convey the fact that the WRF-Chem model with the original GOCART-WRF dust emission scheme (*dust_opt=1*) incorrectly captures strong dust events, which we defined as the cases when AOD > 1.

3) The ALL_OK run was just one of the model realizations. It is not appropriate to treat it as truth and designate the differences from it as biases.

We agree. Here we discuss the effect of changes we introduced in the model. The ALL_OK run is not a ground truth, but differences or biases with respect to this run give us the measure of introduced corrections. We have corrected the text to make this point clear.

4) How useful is the Merra2BC utility in general sense? Since the MERRA-2 reanalysis is essentially a global atmospheric reanalysis generated by an atmospheric circulation model with the incorporation of trace gas constituents and aerosols. It is not a fully coupled atmosphere-chemistry model and I would think that the so created gaseous and aerosol species data may not be as useful as those from fully coupled chemistry models such as MOZART-4.

One of the advantages of the MERRA-2 reanalysis is the fact that it assimilates AOD and correctly produces dust content in the atmosphere. Additionally, MERRA-2 has a higher resolution than MOZART-4. MOZART-4 resolution is 128×64 grid boxes, while MERRA-2 has 576×360. MOZART-4 has 4 dust size bins with a maximum of 5 microns, while MERRA-2 has 5 size bins with a maximum of 20 microns. Besides dust, MERRA-2 calculates sea salt, ozone, sulfate, black and organic carbon, sulfur dioxide, DMS, and MSA. MERRA-2 hourly fields are available from 1980 to present and are an invaluable asset for building initial and boundary

conditions for regional aerosol and chemistry simulations. This is not to diminish the value of MOZART-4's more sophisticated chemistry. But WRF-Chem uses chemical mechanisms and aerosol microphysics quite consistent with MERRA-2, which provides another advantage of using MERRA-2 for building IC&BC for WRF-Chem.

5) The authors mentioned that Figure 4 shows the averaged AOD time-series and scatter plots obtained from the ALL_OK and NON_LOG_046 runs. Instead, I found the spatial patterns of AOD and their differences.

Thank you for capturing the Figure 4 misrepresentation. We have corrected the sentence, which now reads: "*Figure 4 shows the averaged AOD fields obtained from the ALL_OK and NON_LOG_046 runs, as well as their relative bias (%).*"

Reply to the comments of 2nd Referee:

General comments

Comment 1: There are a very large number of appendices, some of them very short, which results in a disjointed manuscript that doesn't flow very well. I would consider reformulating these so that the overall paper flows better (possibly merging those which are fundamental to the paper, e.g. the non-technical description of Merra2BC, into the body). Appendix F doesn't even appear to be referenced anywhere in the manuscript.

We thank the reviewer for the valuable comments.
We have merged Appendix H, which presents the improved numerical scheme for gravitational settling calculations, with the main body of the paper. Appendix F is combined with appendix G and is now referenced in Sect. 3.3. The appendices are specifically designed to consolidate the technical information about diagnostic calculations and pre-processing (Merra2BC). We feel it is convenient to have this information on hand at the end of the main text.

Comment 2:
There are several places (particularly in the introduction, but also in section 2.1.1) where an excessively long list of citations is given to exemplify a point – please consider whether all of these are necessary and if not cite the most pertinent examples.

The reference list in section 2.1.1 has been shortened.

Comment 3:
In a number of places, configuration parameters of WRF-Chem are referred to without explaining their meaning. While the manuscript is obviously of most interest to those familiar with this model, it should be understandable more widely.

We have added Table 1 into the Introduction section, where a short description of the *chem_opt* namelist options affected by our modifications is provided.

Comment 4:
Finally, the experiments carried out should be described prior to the results section.

We have added a description of each found inconsistency into the Introduction section (before Table 1). Although this gives an impression of how the test experiments are organized, we prefer to keep the detailed description of the experiments in the specific sections, as it is combined with the explanation of a specific problem and how it was rectified.

Specific comments:

p.3, lines 29–31: please include a table explaining what these options are.

We have added Table 1 at the end of the Introduction section, where all *chem_opt* options are explained.

p.4, line 14: please state what "chem_opt=300" means.

Table 1 now includes a description of the *chem_opt=300.* The text has also been modified to read: "*We use chem_opt=300 namelist option, which corresponds to simulation using GOCART aerosol module without chemical reactions.*"

p.4, line 24: is AFWA an acronym? If so, please expand on first use.

Acronym AFWA has been expanded in the text into “Air Force Weather Agency”

p.6, lines 28–29: should this be ERA-Interim (not ECMWF Interim)?

This sentence has been changed to read: “*IC&BC for meteorological fields are derived from the ERA-Interim (Dee et al., 2011) global atmospheric reanalysis produced by the European Centre for Medium-Range Weather Forecasts (ECMWF).*”

p.7, lines 9–12: a little more explanation of Merra2BC is warranted in the main body of the paper, especially given that its introduction is later highlighted in the conclusions suggesting it’s more than a minor element.

This has been edited so that we now discuss the rationale of using MERRA-2 output for constructing the IC&BC. MERRA-2 aerosol and chemical species fields are superior (in terms of spatial resolution, time coverage, and because they are constrained by observations) in comparison to those used in WRF-Chem so far for calculation IC&BC (MOZART-4, for example). Merra2BC is a preprocessor that conveniently transforms MERRA-2 output into WRF-Chem IC&BC.

p.7, line 14: this is confusing, because it refers to "all inconsistencies" when these haven’t yet been enumerated in the text. Please reformulate so that the inconsistencies, changes made, and experiments carried out are introduced prior to the results section.

Thank you for your comment. To clarify this issue, a new paragraph has been added into the Introduction section, where we briefly introduce the found inconsistencies and their effects.

p.7, line 30: is it documented that a log-based distribution is the one on which the parameterisation is based, and that therefore this is an inconsistency? Or is it the author’s assumption/assertion that such a distribution is universally the correct one to assume, whatever the parameterisation?

Calculating PM2.5 and PM10 concentrations requires the integration of aerosol volume size distribution over the radius r from 0 to 2.5 um, and from 0 to 10 um, respectively. Integration can be performed assuming that the size distribution is a function of r or ln(r). We calculate coefficients d_25, s_25, d_10 in eq.2 assuming that aerosol size distribution is a function of ln(r). This method is acknowledged in CAMS reanalysis (https://confluence.ecmwf.int/pages/viewpage.action?pageId=153393481) and is justified by the fact that an aerosol size distribution is a smoother function of ln(r) than r, and therefore numerical integration is more accurate.

p.8, line 6: “overestimated” sounds like it is a comparison to observation, but I think this means only in comparison to the modified model? Please make this clear, and if possible illustrate if this is an improvement against relevant observations. (It is not given that a model which appears to be more theoretically correct actually improves results.)

We agree and have clarified the text accordingly. We compare results from two runs, with and without corrections. This is now systematically acknowledged in the text. Although we do not provide any test with observation, bearing in mind previously reported results, our corrections make the WRF-Chem output more consistent with observations.

p.8, line 19: it's not quite true that these are not accounted for - all of DUST1 is included if you add up the coefficients; it's merely that some of it is treated as larger than it should be (and thus less optically effective). Please clarify this in the text.

Thank you for your comment. The dust mass from the DUST1 bin was not omitted but was erroneously mapped onto coarser MOSAIC bin-sizes than required. This resulted in the underestimation of AOD, as discussed in the text. We have now clarified this issue throughout the text.

p.10, lines 3–4: please clarify what you mean here. A "function of natural logarithm of radius" is also a "function of radius". Do you mean specifically a linear function of each?

Not exactly; here we are talking about linear interpolation of a nonlinear function. It could be performed in radius space, or in ln(r) space. We argue that it is more accurate to interpolate in the ln(r) space, as discussed above. The text has been corrected to clarify this issue.

p.14, lines 20, 23, 27: again, "overestimation" suggests this is by reference to some actual measurement rather than to the modefied model - please clarify if this is just "one model version is higher than the other" or if the change is an improvement or degradation compared to measurements.

Thank you, the text has been clarified. Please see our response to comment p.8, line 6. (see above)

p.14, line 29–p.15, line 3: Section 3.4 is very brief – to be meaningful, this needs to show to what extent the contribution from both initial and boundary conditions is significant relative to one another and to sources within the domain.

We show the capability of Merra2BC in constructing IC&BC. ICs are important for making an accurate forecast. BCs impact is seen near the boundaries, and we show how far their signal propagates. The effect of BCs scales with the magnitude of the fluxes through the boundaries of a domain. We can make their effect stronger but that is not the point. The advantage of accurately calculated IC&BS is that they allow for improvements in such things as air-quality forecasts, and in many cases, for reliable use of a smaller domain, when the signal from boundaries is well defined.

p.16, line 9: as above, please clarify that submicron particles aren't omitted as such, but treated incorrectly.
This issue has been clarified. Please see our response to comment p8, line19 (see above).

p.18, line 9: is it really correct that MERRA-2 has a globally-uniform constant surface pressure of 1000hPa? That seems highly unlikely in a meteorological reanalysis – please check and clarify, as this is what the current text suggests.
Thank you for pointing this out, the sentence in question has been deleted.

p.19, Figure A2: both singular and plural should be "species" (not "specie").
Thank you, this has been corrected.

p.21, lines 7–11: please state the AERONET wavelength(s) from which these calculations are performed to generate the 550nm value.

We use a 440-675 nm wavelength range. The text has been modified to state this.

Improving dust simulations in WRF-Chem model v4.1.3 coupled with GOCART aerosol module

Alexander Ukhov[1], Ravan Ahmadov[2,3], Georg Grell[3], and Georgiy Stenchikov[1]

[1]King Abdullah University of Science and Technology, Division of Physical Sciences and Engineering, Thuwal, Saudi Arabia
[2]CIRES, University of Colorado, Boulder, CO, USA
[3]NOAA Earth System Research Laboratory, Boulder, CO, USA

Correspondence: Alexander Ukhov (alexander.ukhov@kaust.edu.sa)

Abstract. In this paper, we rectify inconsistencies that emerge in the WRF-Chem v3.2 code when using the Goddard Chemistry Aerosol Radiation and Transport (GOCART) aerosol module. These inconsistencies have been reported, and corrections have been implemented in WRF-Chem v4.1.3. Here, we use a WRF-Chem experimental setup configured over the Middle East (ME) to estimate the effects of these inconsistencies. Firstly, we show that the diagnostic output ~~of~~ underestimated $PM_{2.5}$ surface concentration ~~was underestimated~~ by 7% and overestimated PM_{10} ~~was overestimated~~ by 5%. Secondly, we demonstrate that the contribution of sub-micron dust particles was ~~underestimated~~ incorrectly accounted for in the calculation of optical properties, and thus, Aerosol Optical Depth (AOD) was ~~consequently~~ underestimated by 25-30%. Thirdly, we show that ~~an inconsistency in the process of gravitational settlingled to the overestimation of the~~ gravitational settling, as it was coded, overestimated dust column loadings by 4-6%, PM_{10} surface concentrations by 2-4%, and the rate of ~~dust gravitational~~ gravitational dust settling by 5-10%. We present ~~a methodology to calculate diagnostics that can be~~ the methodology for calculating diagnostics we used to estimate the ~~effects of these applied changes. Our corrections also help to explain the overestimation of PM_{10} surface concentrations encountered~~ impacts of introduced code modifications. Our results explain why in many WRF-Chem simulations ~~. We also~~ PM_{10} concentrations were exaggerated. We share the developed *Merra2BC* interpolator, which allows processing Modern-Era Retrospective Analysis for Research and Applications, Version 2 (MERRA-2) output for constructing initial and boundary conditions for chemical species~~and aerosols based on MERRA-2 reanalysis. The results of this work can be useful for those who simulate the dust cycle using the WRF-Chem model coupled with the GOCART aerosol module.~~ , and aerosols.

1 Introduction

~~Global dust emissions estimated to be in range 1000 to 2000 (Zender et al., 2004). The Middle East (ME) and North Africa contribute about half of the dust emissions on a global scale (Prospero et al., 2002). Situated in the center of the northern subtropical dust belt, the Arabian Desert is the third largest region for dust generation after the Sahara and the East Asian deserts. The most significant dust sources of the ME include the Al-Nafud desert (40° E–45° E; 27° N–29° N), the Rub Al-Khali desert (44° E–56° E; 16° N–23° N), the Al-Dahna desert (45° E–48° E; 25° N–28° N), the dust source region between 22° N to 25° N, and the roughly 50 km-wide stretch of land along the west coast of the Arabian Peninsula; see Fig. 1.~~

~~Frequent dust storms lift millions of tons of dust into the atmospheric boundary layer. Results of the modeling presented in (Kalenderski et al., 2013) show that a typical dust storm over the ME emits ~18 of dust over several days. The ME is also subjected to the inflow of dust from the nearby Sahara Desert, which is another major dust source region (Osipov et al., 2015; Kalenderski an~~

~~.~~

Produced by wind erosion, mineral dust is one of the major drivers of climate over the ME. Dust suspended in the atmosphere affects the energy budget by absorbing and scattering incoming solar radiation ~~(Sokolik and Toon, 1996; Miller and Tegen, 1998; Kalenders~~ (Sokolik and Toon, 1996; Miller and Tegen, 1998; Kalenderski et al., 2013; Osipov et al., 2015; Osipov and Stenchikov, 2018) and by affecting cloud radiative properties (Levin et al., 1996; Forster et al., 2007; Rotstayn and Lohmann, 2002). ~~Calculations conducted by Kalenderski et al. (2013) clearly indicated that the presence of dust in the atmosphere causes a significant reduction of solar radiation reaching the earth's surface; for example, they calculated surface cooling under a dust plume during a dust storm of 100 .~~

Dust can also negatively impact infrastructure and technology. For instance, ~~reduced~~ reducing solar radiation reaching the earth's surface dust decreases the output of photo-voltaic systems. Moreover, dust deposition on solar panels deteriorates their efficiency (Mani and Pillai, 2010; Rao et al., 2014; Sulaiman et al., 2014).

Dust also has socioeconomic implications. Bangalath and Stenchikov (2015) showed that due to ~~the~~ high dust loading, the tropical rain belt across ~~Middle East~~ the ME and North Africa strengthens and shifts northward, causing up to a 20% increase in summer precipitation over the semi-arid strip south of the Sahara, including the Sahel.

~~Background dust loading over the ME is higher relative to other parts of the world (Jish Prakash et al., 2015; Kalenderski et al., 2013) . High values of dust loading correspond to the high values of aerosol optical depth (AOD). Osipov et al. (2015) and Kalenderski and Stench showed that over the ME mineral dust is the major contributor to the AOD (~87).~~

Frequent dust outbreaks have a profound effect on air quality in the ME region (Cahill et al., 2017; Banks et al., 2017; Farahat, 2016; Kalenderski and Stenchikov, 2016; Munir et al., 2013; Alghamdi et al., 2015; Lihavainen et al., 2016; Anisimov et al., 2017). Air pollution is characterized by near-surface concentrations of particulate matter (PM), which comprise both $PM_{2.5}$ and PM_{10} (particles with diameters less than 2.5 μm and 10 μm, respectively). ~~Similarly to AOD, dust~~ Dust is the major contributor to PM over the ME region ~~. Annually averaged (2015-2016) $PM_{2.5}$ and PM_{10} near-surface concentrations over the Arabian Peninsula were up to 15 times higher than the World Health Organization (WHO) guidelines (Ukhov et al., 2020a). Karagulian et al. (2019) used the WRF-Chem model (Skamarock et al., 2005; Grell et al., 2005; Powers et al., 2017) to simulate a dust storm over the UAE on 2 April, 2015, when the simulated PM_{10} concentrations peaked at 1500 . During another severe dust storm that occurred on 18-22 March, 2012, the AOD reached 4.5 at the *KAUST Campus* AErosol RObotic NETwork (AERONET; Holben et al. (1998)) station (Jish Prakash et al., 2015). This dust storm covered a huge area, including Iraq, Iran, Kuwait, Syria, Jordan, Israel, Lebanon, UAE, Qatar, Bahrain, Saudi Arabia, Oman, Yemen, Sudan, Egypt, Afghanistan, and Pakistan. Dust source regions along the western coast of the Arabian Peninsula were also activated. The dust emission rate calculated by the WRF-Chem model exceeded 500 (Jish Prakash et al., 2015).~~

~~Dust is an important contributor to the fertilization of phytoplankton (Watson et al., 2000). Dust deposition provides nutrients to~~ (Ukhov et al., 2020a). The ME is also subjected to the inflow of dust from the nearby Sahara Desert, which is another major

dust source region (Osipov et al., 2015; Kalenderski and Stenchikov, 2016). Dust deposition fertilizes ocean surface waters and the seabed ~~(Talbot et al., 1986; Swap et al., 1996; Zhu et al., 1997). Jish Prakash et al. (2015) used modeling to estimate the annual dust deposition to the Red Sea via major dust storms to be 6 . Simulations conducted in Anisimov et al. (2017) suggested that the dust contribution from the Red Sea coastal area to the total deposition flux into the Red Sea could be substantial. Jish Prakash et al. (2016); Engelbrecht et al. (2017) measured an average dust deposition rate along the Red Sea coast of Saudi Arabia of ≈14 per month, with lowest deposition rates in winter and increased deposition rates during August to October. Furthermore, the authors conducted X-ray diffraction analysis of deposited dust samples, and found variable amounts of quartz, feldspars, micas, and halite, with lesser amounts of gypsum, calcite, dolomite, hematite, and amphibole. The information presented in those studies can be used as a proxy to estimate nutrient input into the Red Sea and impact on health.~~ (Watson et al., 2000; Talbot et al., 1986; Swap et al., 1996; Zhu et al., 1997).

~~Osipov and Stenchikov (2018) showed that the dust radiative effect has a profound thermal and dynamic impact on the Red Sea, whereby dust cools the Red Sea, reduces the surface wind speed, and weakens both the exchange at the Bab-el-Mandeb strait and the overturning circulation.~~

Thus, given the impact of dust on climate, ~~ecosystems, and~~ technology, human health, and ecosystems, an accurate description of ~~these~~ dust effects in numerical ~~weather prediction~~ models is essential~~, requiring careful numerical simulation~~. In the first place, it requires careful description of the dust cycle~~, from emission from~~ ; from emission at the earth's surface, to transport in the atmosphere, and, finally, to removal by deposition.

Most of the studies mentioned above were ~~produced by~~ conducted within the group of Atmospheric and Climate Modeling at King Abdullah University of Science and Technology (KAUST) using the WRF-Chem model (Skamarock et al., 2005; Grell et al., 2005; Po . WRF-Chem is a popular open-source tool that is widely used to study atmospheric chemistry, air quality, and aerosols (Jish Prakash et al., 2015; Khan et al., 2015; Kalenderski et al., 2013; Kalenderski and Stenchikov, 2016; Parajuli et al., 2019; Anisimov et al., 2017; Osipov and Stenchikov, 2018). This model has been used extensively to study aerosols and their impact on air quality ~~(Fast et al., 2006; Wang et al., 2015; Fast et al., 2009; Ukhov et al., 2020a, b), climate at the regional scales~~ (Fast et al., 2006; Wang et al., 2015; Fast et al., 2009; Ukhov et al., 2020a, b; Parajuli et al., 2020), climate (Zhao et al., 2010, 2011; Chen et al., 2014; Fast et al., 2006), and to analyse dust outbreaks (Bian et al., 2011; Chen et al., 2014; Fountoukis et al., 2016; Ma et al., 2019; LeGrand et al., 2019; Su and Fung, 2015; Chen et al., 2018; Eltahan et al., 2018; Bukowski and van den Heever, 2020) in ~~Middle East~~ the ME and North Africa (Zhang et al., 2015; Flaounas et al., 2016; Rizza et al., 2017; Karagulian et al., 2019; Rizza et al., 2018), North America (Zhao et al., 2012), India (Dipu et al., 2013; Kumar et al., 2014), and ~~in~~ Australia (Nguyen et al., 2019). ~~Most of the aforementioned papers used~~ Many aforementioned studies utilized the WRF-Chem model coupled with the Goddard Chemistry Aerosol Radiation and Transport (GOCART) aerosol module (Chin et al., 2002). The GOCART module simulates major tropospheric aerosol components, including sulfate, dust, black and organic carbon, and sea-salt, and includes algorithms for dust and sea salt emissions, dry deposition, and gravitational settling. The GOCART module is one of the most popular aerosol modules used in WRF-Chem (Bian et al., 2011; Dipu et al., 2013; Kumar et al., 2014; Chen et al., 2014; Su and Fung, 2015; Zhang et al., 2015; Flaounas et al., 2016; Fountoukis et al., 2016; Rizza et al., 2017; Flaounas et al., 2017; Nabavi et al., 2017; Chen et al., 2018; Rizza et al., 2018; Ma et al., 2019; LeGrand

et al., 2019; Parajuli et al., 2019; Yuan et al., 2019; Ukhov et al., 2020a; Eltahan et al., 2018; Nguyen et al., 2019; Bukowski and van den Heever, 2020).

However, working with the WRF-Chem/Gocart modeling system we found a few ~~discrepancies~~ inconsistencies in the physical parameterizations ~~that affected WRF-Chem performancewhen used with the GOCART module. The following are the~~ which affected its performance. Firstly, we found that the diagnostic output of $PM_{2.5}$ and PM_{10} was miscalculated. Secondly, the contribution of sub-micron dust particles was underestimated and thus, aerosol optical depth (AOD) was underestimated. Thirdly, an inconsistency in the process of gravitational settling was leading to a violation of the dust and sea salt mass balance. The complete list of the WRF-Chem *chem_opt* namelist options that were affected ~~: *GOCARTRACM_KPP, MOZCART_KPP, RADM2SORG, DUST, GOCART_SIMPLE, RACM_ESRLSORG_AQCHEM_KPP, GOCARTRADM2, RADM2SORG_AQ, RADM2SORG_A RACMSORG_AQCHEM_KPP*. All these discrepancies affected the~~ are presented in Tab. 1.

Table 1. WRF-Chem *chem_opt* namelist options.

		Found inconsistencies in calculation of		
chem_opt	Description	PM	Optical properties	Gravitational settling
2	MADE/SORGAM aerosols, RADM2 chemistry	-	-	+
11	same as *chem_opt*=2 and some aqueous reactions	-	-	+
41	same as *chem_opt*=2 and aqueous reactions	-	-	+
42	same as *chem_opt*=41 using KPP library	-	-	+
109	MADE/VBS aerosols, RACM Chemistry and aqueous reactions using KPP library.	-	-	+
112	GOCART aerosols, MOZART Chemistry using KPP library.	+	+	+
300	GOCART aerosols, no ozone chemistry.	+	+	+
301	GOCART aerosols, RACM chemistry using KPP library.	+	+	+
303	GOCART aerosols, RADM2 chemistry	+	+	+
401	Dust concentration only	-	-	+

All of these inconsistencies have affected WRF-Chem performance since April 2, 2010, when the WRF-Chem v3.2 was released. We have reported all ~~these discovered issues, which~~ those issues, and they have been rectified in the WRF-Chem v4.1.3 code release. In this paper, we specifically discuss these ~~discrepancies and~~ corrections and evaluate how they have affected ~~previously reported~~ results. We ~~also~~ demonstrate the methodology ~~to calculate the~~ for calculating diagnostics that we used to estimate the ~~effect~~ impact of the introduced ~~changes in the code~~corrections. We also share with the community the *Merra2BC* interpolator (Ukhov and Stenchikov, 2020), which allows constructing initial and boundary conditions (IC&BC) for chemical species and aerosols using MERRA-2 reanalysis (Randles et al., 2017). We believe that this discussion is in ~~the spirit of the~~ line with the open-source ~~movement~~ paradigm and will help users to better handle the code, understand physical links, and evaluate the sensitivity of the results to particular physical assumptions made in the code. ~~Another purpose of this paper is to increase awareness to WRF-Chem users of the changes we have made to the WRF-Chem code.~~

The paper is organized as follows: Section 2 describes the WRF-Chem model setup. In Section 3, a description of the inconsistencies found in the WRF-Chem code and their effects on the results are presented. Conclusions are presented in Section 4.

2 WRF-Chem experimental setup

~~The WRF-Chem experimental setup provided below demonstrates the methodology, which was adopted by the KAUST group to simulate~~ To quantify the effects of introduced code modifications, we use our typical model setup which we previously adopted for simulating dust emissions using the WRF-Chem model coupled with the GOCART aerosol module. The WRF-Chem simulation domain (see Fig. 1) is centered at 28°N, 42°E, with a 10 km×10 km horizontal grid (450×450 grid nodes). The vertical grid comprises 50 vertical levels with enhanced resolution closer to the ground. The model top boundary is set at 50 hPa. We use ~~the~~ *chem_opt*=300 namelist option, which corresponds to simulation using GOCART aerosol module ~~*chem_opt*=300.~~ without ozone chemistry.

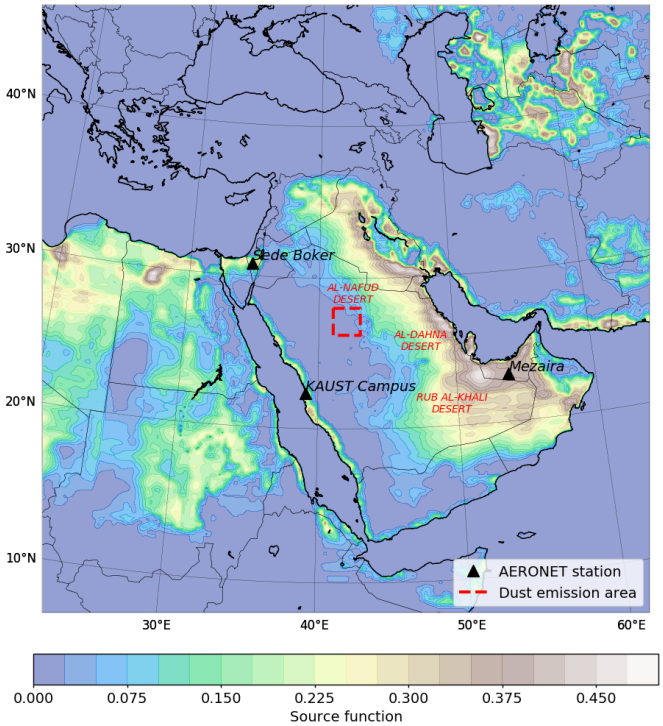

Figure 1. Simulation domain with marked locations of the AERONET sites. The red square corresponds to dust emission area. Shaded contours correspond to source function S (Ginoux et al., 2001).

~~We used the following set of physical parameterizations.~~ The Unified Noah land surface model (*sf_surface_physics*=2) and the Revised MM5 Monin-Obukhov scheme (*sf_sfclay_physics*=1) are chosen to represent land surface processes and surface

layer physics. The Yonsei University scheme is chosen for PBL parameterization (*bl_pbl_physics*=1). The WRF single moment microphysics scheme (*mp_physics*=4) is used for the treatment of cloud microphysics. The New Grell scheme (*cu_physics*=5) is used for cumulus parameterization. The Rapid Radiative Transfer Model (RRTMG) for both short-wave (*ra_sw_physics*=4) and long-wave (*ra_lw_physics*=4) radiation is used for radiative transfer calculations. Only the aerosol direct radiative effect is accounted for. More details on the physical parameterizations used can be found at http://www2.mmm.ucar.edu/wrf/users/phys_references.html.

~~There are three GOCART compatible dust emission schemes available for the~~ Dust size distribution in the GOCART module is approximated by five dust bins; see Tab. 2. Dust density is assumed to be 2500 $\mathrm{kg/m^3}$ for the first dust bin and 2650 $\mathrm{kg/m^3}$ for dust bins 2-5.

In WRF-Chem ~~model~~there are three dust emission schemes that can be used with GOCART: the original GOCART-WRF scheme (*dust_opt*=1) (Bagnold, 1941; Belly, 1964; Gillette and Passi, 1988), the ~~AFWA~~ Air Force Weather Agency (AFWA) scheme (*dust_opt*=3) (Marticorena and Bergametti, 1995; Su and Fung, 2015; Wang et al., 2015), and the University of Cologne (UoC) scheme (*dust_opt*=4) (Shao, 2001, 2004; Shao et al., 2011). The detailed description of all schemes is ~~also~~ provided in LeGrand et al. (2019).

Table 2. Radii ranges (μm) of dust and sea salt bins used in the GOCART aerosol module.

	Bin				
	1	2	3	4	5
Dust	0.1-1.0	1.0-1.8	1.8-3.0	3.0-6.0	6.0-10.0
Sea salt	0.1-0.5	0.5-1.5	1.5-5.0	5.0-10.0	-

Here, we simulate dust emissions using the original GOCART-WRF scheme (*dust_opt*=1) ~~. Dust and sea salt size distributions in WRF-Chem GOCART module are approximated by five dust and four sea-salt size bins; see Tab. 2. Dust density is assumed to be 2500 for the first dust bin and 2650 for dust bins 2-5. Sea salt density is 2200 . Emission of sea salt is calculated according to Gong (2003). Dust emission from the surface is calculated using the emission scheme~~ proposed in Ginoux et al. (2001). Dust emission mass flux, F_p ($\mathrm{\mu g\ m^{-2}\ s^{-1}}$) in each dustbin p=1,2,...,5 is defined by the relation:

$$F_p = \begin{cases} CSs_p u_{10m}^2 (u_{10m} - u_t), & \text{if } u_{10m} > u_t \\ 0, & \text{if } u_{10m} \leq u_t \end{cases} \quad (1)$$

where, C ($\mathrm{\mu g\ s^2\ m^{-5}}$) is a spatially uniform factor which controls the magnitude of dust emission flux; S is the source function (Ginoux et al., 2001) (see Fig. 1) that characterizes the spatial distribution of dust emissions; u_{10m} is the horizontal wind speed at 10 m; u_t is the threshold velocity, which depends on particle size and surface wetness; s_p is a fraction of ~~mass emitted into~~ dust emission mass flux within dustbin p.

~~Simulation domain with marked locations of the AERONET sites. The red square corresponds to dust emission area. Shaded contours correspond to source function S (Ginoux et al., 2001).~~ Sea salt size distribution in the GOCART module is approximated by four sea-salt bins (see Tab. 2). Sea salt density is 2200 $\mathrm{kg/m^3}$. Emission of sea salt is calculated according to Gong (2003).

2.1 Dust emission tuning

~~Before the production run, dust emissions are typically tuned, where the dust emission~~ To adjust to regional conditions, dust emission in the model is calibrated to fit observed AOD and ~~aerosols~~ aerosol volume size distributions (AVSD) obtained from the ~~AERONET AOD measurements and retrievals~~AErosol RObotic NETwork (AERONET; Holben et al. (1998)). AERONET AOD observations represent the total AOD with contributions from all types of aerosols. But because in the ME dust is more prevalent than all other aerosols, we focus on dust emission only. More detailed information on dust emission tuning is provided in Ukhov et al. (2020a). For this study, we ~~have chosen~~ choose three AERONET sites: *KAUST Campus*, *Mezaira*, and *Sede Boker* located within the domain (Fig. 1). We ~~utilized~~ utilize level 2.0 (cloud screened and quality assured) AERONET AOD data. ~~From here forward, we will presume~~ Note that from here onwards, we assume that AOD is given or calculated at 550 nm; see Appendix C.

2.1.1 Tuning the C parameter

~~As in our previous studies Kalenderski et al. (2013); Jish Prakash et al. (2015); Khan et al. (2015); Kalenderski and Stenchikov (2016); An and in other studies Zhao et al. (2010, 2013); Kumar et al. (2014); Flaounas et al. (2016); Fountoukis et al. (2016); Flaounas et al. (2017); , we tune dust emissions to fit the AOD from the AERONET measurements. For this purpose, the parameter~~ To adjust dust emissions we first tune the C factor from Eq. 1~~has been adjusted to achieve the best~~ , as practiced in our own studies (Kalenderski et al., 2013; Jish Prakash et al., 2015; Khan et al., 2015; Kalenderski and Stenchikov, 2016; Anisimov et al., 2017; Parajuli e and in the studies of other authors (Zhao et al., 2013; Kumar et al., 2014; Flaounas et al., 2017; Rizza et al., 2017). Our test runs indicate that for the ME, $C = 0.5$ achieves a good agreement between simulated and observed AOD at the *KAUST Campus, Mezaira*, and *Sede Boker* AERONET sites. ~~As determined during test runs, a~~ Therefore this sub-optimal value C ~~of~~ = 0.5 is ~~kept constant~~ retained in all subsequent ~~production~~ runs.

2.1.2 Tuning the s_p ~~parameter~~fractions

We also tune s_p fractions from Eq. 1 to better reproduce the AVSDs provided by AERONET retrievals using the spectral deconvolution algorithm (SDA) (O'Neill et al., 2003). The AERONET ~~retrieval algorithm~~ provides column integrated AVSD $dV/d\ln r$ ($\mu\mathrm{m}^3/\mu\mathrm{m}^2$) on 22 logarithmically equidistant discrete points in the range of radii between 0.05 and 15 µm. ~~We~~ For AVSDs we use the AERONET V3, level 2.0 product (Dubovik and King, 2000).

In WRF-Chem the default values of parameter s_p from Eq. 1 are $\{0.1, 0.25, 0.25, 0.25, 0.25\}$, for the $DUST_1$, $DUST_2$, ..., $DUST_5$ dust bins, respectively. ~~Our preliminary runs indicated that using~~ They control the size distribution of emitted dust.

Our test runs indicate that when we use the default s_p values ~~WRF-Chem produced~~ the dust volume size distributions ~~that did~~ in the atmosphere do not match those from AERONET. To achieve a better agreement between the modeled and AERONET volume size distributions, we ~~adjusted~~ adjust the fractions s_p ~~. We obtained the following s_p values during the preliminary runs:~~ to be {0.15, 0.1, 0.25, 0.4, 0.1}. ~~These values~~ The fractions s_p are set in the *phys/module_data_gocart_dust.F* file, array $frac\_s$. We effectively increase the dust emission in the finest $DUST_1$ and in coarse $DUST_4$, and decrease those in $DUST_2$ and $DUST_5$. The size distribution of emitted dust is further processed in the atmosphere.

2.2 Initial and boundary conditions for meteorological parameters, chemical species, and aerosols

As is the case with any partial differential equation solver, WRF-Chem requires ~~to set~~ the IC&BC for meteorological parameters and chemical species. IC&BC for meteorological fields are derived from the ERA-Interim (Dee et al., 2011) global atmospheric reanalysis produced by the European Centre for Medium-Range Weather Forecasts ~~-Interim data set (Dee et al., 2011)~~(ECMWF). IC&BC for chemical species are ~~needed~~ required to account for initial concentrations and inflow ~~concentrations~~of aerosols and chemical species. The setting of improper lateral boundary conditions for ~~chemical species~~ aerosols and chemistry may significantly affect the result of the simulation~~where there is a case of strong inflow of chemicals through the boundaries~~. The role of lateral boundary conditions increases if the domain is located close to a significant source of dust or other ~~chemical species or aerosols. In this case, chemical species concentrations~~ chemicals. Concentrations of aerosols and chemicals within the domain ~~will be strongly~~ are especially affected by the inflow through the lateral boundaries of species with long atmospheric lifetimes~~through the lateral boundaries~~.

By default, WRF-Chem uses ~~an~~ the idealized vertical profiles ~~for~~ of a limited number of chemical species for calculating IC&BC. These profiles are obtained from the NALROM model (Liu et al., 1996) simulation and ~~based upon~~ are representative of the northern hemispheric, mid-latitude (North America) summer and clean ~~environment conditions, and covers the lower troposphere~~environmental conditions. Another option in WRF-Chem is to use the output from the ~~MOZART-4 (The~~ Model for Ozone And Related chemical Tracers, version 4 (MOZART-4) global model (Emmons et al., 2010), which is an offline tropospheric global chemical transport model~~particularly suited for studies of the troposphere~~.

~~Since the Arabian Peninsula is affected by the inflow of dust from the Sahara (Kalenderski and Stenchikov, 2016), using proper boundary conditions is important. For this purpose, we developed~~ The MERRA-2 reanalysis (Randles et al., 2017) provides a consistent distribution of aerosols and chemical species constrained by observations with the spatial resolution about 50 km. MERRA-2 aerosol and chemical fields are superior compared to those used previously in WRF-Chem. To calculate the chemical IC&BC using MERRA-2 output, we develop an interpolator *Merra2BC* (Ukhov and Stenchikov, 2020), which uses gaseous and aerosol ~~collection~~ fields from MERRA-2 reanalysis ~~(Randles et al., 2017)~~ to construct the IC&BC required by the WRF-Chem simulation. For more details regarding the *Merra2BC* interpolator, see Appendix A.

3 Results

In the discussion below, we refer to the WRF-Chem run with all inconsistencies fixed and with properly adjusted dust emission (see ~~See~~Sect. 2.1), with IC&BC constructed using the developed *Merra2BC* interpolator (see ~~See~~Sect. 2.2) as *ALL_OK*.

~~The~~ To quantify the effect of each inconsistency ~~found in the code is demonstrated in the corresponding~~ we perform a WRF-Chem run ~~, where all other inconsistencies are rectified except the one that we are focused on at~~ where all the other corrections we discuss here are implemented, with the exception that we focus on a given time. The relative ~~bias of some quantity~~ anomaly (%) of a specific set of variables in this run with respect to the *ALL_OK* run is ~~calculated and the comparison with *ALL_OK* run is provided~~presented as a measure of sensitivity to the chosen correction. All WRF-Chem runs are performed for 1-12 August, 2016.

3.1 Calculation of $PM_{2.5}$ and PM_{10}

The subroutine *sum_pm_gocart* in *module_gocart_aerosols.F* calculates $PM_{2.5}$ and PM_{10} surface concentrations using the following formulas:

$$\begin{aligned} PM_{2.5} &= \rho \cdot (DUST_1 + DUST_2 \cdot d\_25 + SEAS_1 + SEAS_2 \cdot s\_25), \\ PM_{10} &= \rho \cdot (DUST_1 + DUST_2 + DUST_3 + DUST_4 \cdot d\_10 + SEAS_1 + SEAS_2 + SEAS_3), \end{aligned} \quad (2)$$

where ρ is the dry air density ($\mathrm{kg/m^3}$), $DUST_{1,2,3,4}$ and $SEAS_{1,2,3}$ are the mixing ratios ($\mu\mathrm{g/kg}$) of the dust in the first four bins and sea-salt in the first three bins, respectively. The contribution of the dust and sea salt bins to $PM_{2.5}$ and PM_{10} is defined by the mapping coefficients d_25, d_10 for ~~the $DUST_2$, $DUST_4$ dust bins~~ dust and s_25 for ~~the $SEAS_2$ sea saltbin. There are also contributions of black~~ sea salt, see eq. 2. Black and organic carbon and sulfate also contribute to PM, but ~~we omit these contributions~~ their contributions are small in comparison to dust and sea salt, and we omit them for the sake of brevity. ~~We determined that s_25, d_25, d_10 coefficients were calculated incorrectly. We recalculated them assuming~~

We calculate the mapping coefficients using the assumption that dust and sea salt ~~bin concentrations~~ volume size distributions are functions of ~~the~~ natural logarithm of particle ~~radii. Hence, taking into account radii ranges for dust and sea salt bins presented in Tab. 2, the~~ radius. The updated values of mapping coefficients s_25, d_25, d_10 ~~coefficients along with the~~ along with their default values are presented in Tab. 3. Effectively, the contributions in $PM_{2.5}$ of sea salt $SEAS_2$ decreases, while that of dust $DUST_2$ increases. The contribution of $DUST_2$ in PM_{10} decreases. We are not certain how the default coefficients are calculated, but interpolation in the logarithm space is more accurate than in the radius space, as aerosol size distributions are smoother functions of logarithm than radius.

~~We estimated the effect of using default and updated coefficients in PM calculation using *ALL_OK* run. The results~~ The effects of using the updated mapping coefficients in place of default ones in PM calculation are shown in Fig. 2. We ~~calculated~~ calculate the $PM_{2.5}$ and PM_{10} ~~fields of surface concentrations~~ concentrations in the lowest model layer using Eq. 2. Surface concentrations of dust and sea salt are computed using the procedure presented in Appendix E. ~~Using the default~~ When using

Table 3. Default and updated values of s_25, d_25, d_10 mapping coefficients used to calculate $PM_{2.5}$ and PM_{10}.

	Default coefficients	Updated coefficients
s_25	0.942	ln(2.5/1) / ln(3/1) =0.834
d_25	0.286	ln(2.5/2) / ln(3.6/2) =0.380
d_10	0.870	ln(10/6) / ln(12/6) =0.737

the default mapping coefficients values, the model underestimates $PM_{2.5}$ ~~was underestimated~~ by 7% and overestimates PM_{10} ~~was overestimated~~ by 5% ~~, on average~~ on average over the ME.

3.2 Calculation of ~~aerosol~~ Aerosol optical ~~properties~~Properties

For modeling in the ME, the treatment of optically active dust within the model is vitally important. AOD is calculated based on aerosol ~~concentrations~~ number-density and aerosol optical properties, which depend ~~upon~~ on the aerosol size ~~distribution~~ and refractive index. In WRF-Chem, a ~~parameterization (Ghan and Zaveri, 2007) of the Mie theory~~ parameterized Mie theory (Ghan and Zaveri, 2007) is employed to calculate the aerosol optical properties. This parameterization ~~was~~ is modified for the sectional representation of the aerosol size distribution by Fast et al. (2006) and Barnard et al. (2010)~~. In particular,~~ , so the Mie subroutine requires input ~~defined on eighth bins~~of dust number-density or concentration in eight size intervals: {0.039-0.078, 0.078-0.156, 0.156-0.312, 0.312-0.625, 0.625-1.25, 1.25-2.5, 2.5-5.0, 5.0-10.0} µm. These size ~~ranges are used in MOZAIC aerosol module , which is also available in WRF-Chem~~intervals are identical with those used in the Model for Simulating Aerosol Interactions and Chemistry (MOSAIC) microphysical module (Zaveri et al., 2008). Therefore, we ~~refer to these size ranges as MOZAIC bins ($MOZ_{1,2,3,4,5,6,7,8}$~~further refer to them as MOSAIC bins ($MOS_{1,2,3,4,5,6,7,8}$).

~~We implemented~~ To correctly calculate the dust optical properties we implement two corrections in the subroutine *optical_prep_gocart()* in *module_optical_averaging.F* ~~. This subroutine~~ that computes the volume-averaged refractive index needed ~~by the~~ for Mie calculations.

3.2.1 Effect of ~~small particles~~Small Particles

In WRF-Chem's GOCART aerosol module, ~~the radii range of dust particles spans across~~ dust particle sizes span two orders of magnitude, from 0.1 to 10 µm; see Tab. 2. However, we ~~found~~ find that dust particles with radii between 0.1 and 0.46 µm ~~were not~~ are incorrectly accounted for in the Mie calculations of aerosol optical properties. Their mixing ratio is mapped on coarser MOSAIC bins than is required. Since finer particles have a stronger effect on AOD per unit mass in comparison ~~with the~~ to coarser particles, ~~this eventually led to the underestimation of the AOD . Therefore,~~ the ~~model erroneously pushed~~ model AOD is underestimated. As a result, when tuning dust emission we push the model to emit more dust into the atmosphere, in order to fit the observed AOD. We ~~rectified~~ rectify this error by ~~accounting for particles with radii $\geq$0.1 , where 0.1 corresponds to the beginning of the first GOCART dust bin;~~ correcting mapping fractions of $DUST_1$ into MOSAIC bins, see Tab. ~~2~~4.

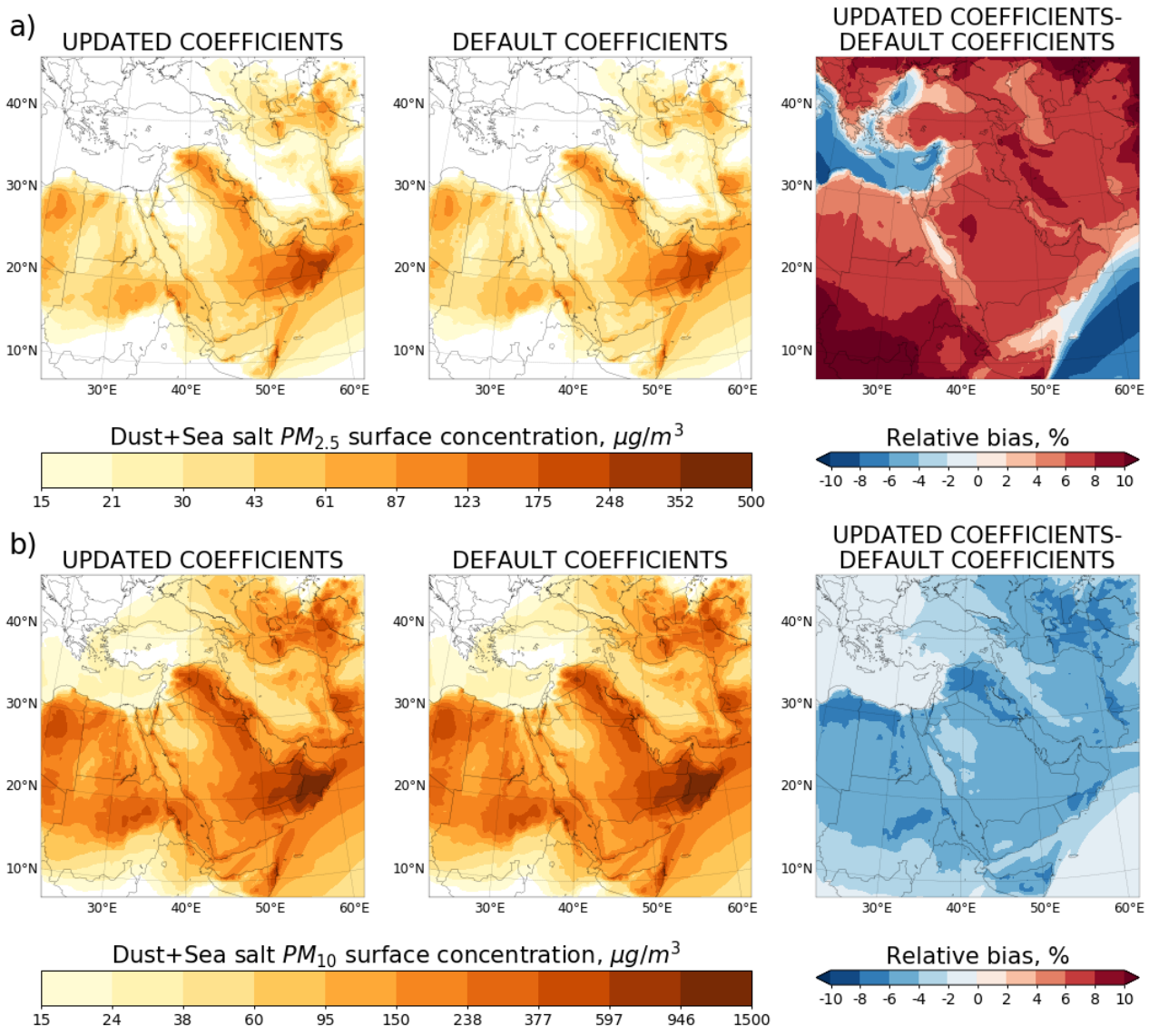

Figure 2. Average dust and sea salt $PM_{2.5}$ a) and PM_{10} b) surface concentration ($\mu g/m^3$) calculated using default and updated coefficients values and relative bias.

~~The effect of these changes is presented in~~ Tab. 4 ~~, where the mass redistribution between~~ presents the mapping fractions of the GOCART dust bins (~~$DUST_{1,2,3,4,5}$) and MOZAIC bins ($MOZ_{1,2,3,4,5,6,7,8}$~~ $DUST_{1,2,3,4}$) to the MOSAIC bins ($MOS_{1,2,3,4,5,6,7,8}$) before and after correction~~is shown.~~ . We do not include in the Tab. 4 GOCART dust bin $DUST_5$ since it is out of the MOSAIC size range and is therefore not accounted for in the mass redistribution. Also, the mass from $DUST_4$ is only partially accounted for. Although this is a potential drawback, it does not impact the AOD drastically, as large particles contribute little in dust AOD. After the changes, the dust mass from $DUST_1$ bin ~~redistributes between $MOZ_{3,4,5,6}$ bins, which cover finer particles.~~

Table 4. Dust mass redistribution between GOCART and ~~MOZAIC~~ MOSAIC bins. Before a) and after b) inclusion of dust particles with radii $\geq$0.1 µm into calculation of aerosol optical properties.

a)						
	~~MOZ_1~~ MOS_1	~~MOZ_2~~ MOS_2	~~MOZ_3~~ MOS_3	~~MOZ_4~~ MOS_4	~~MOZ_5~~ MOS_5	~~MO~~
$DUST_1$	0.0	0.0	0.0	0.0	0.305	
$DUST_2$	0.0	0.0	0.0	0.0	0.0	
$DUST_3$	0.0	0.0	0.0	0.0	0.0	
$DUST_4$	0.0	0.0	0.0	0.0	0.0	
~~$DUST_5$ 0.0 0.0 0.0 0.0 0.0 0.0 0.0 0.0~~ height	b)					
$DUST_1$	0.0	0.0	0.062	0.174	0.347	
$DUST_2$	0.0	0.0	0.0	0.0	0.0	
$DUST_3$	0.0	0.0	0.0	0.0	0.0	
$DUST_4$	0.0	0.0	0.0	0.0	0.0	
~~$DUST_5$ 0.0 0.0 0.0 0.0 0.0 0.0 0.0 0.0~~ height						

~~Before changes, mass was redistributed only between $MOZ_{5,6}$~~ is redistributed between finer $MOS_{3,4,5,6}$ bins compared to the original WRF-Chem where all $DUST_1$ mixing ratio was mapped on the coarser $MOS_{5,6}$ bins.

3.2.2 Bin ~~concentration interpolation~~Concentration Interpolation

~~We also found that~~ Originally, the subroutine *optical_prep_gocart()* redistributes dust and sea salt mass from ~~the GOCART into the MOZAIC binsassuming that bin concentrations are functions~~ GOCART into MOSAIC bins, using the assumption that dust size distribution is a function of particle radius. ~~Consistently with Sec~~Consistent with Sect. 3.1, here we conduct interpolation ~~here assuming that bin concentrations are functions~~ assuming that dust distribution is a function of natural logarithm of radius. This correction causes changes in the mass redistribution between the GOCART and ~~MOZAIC~~ MOSAIC bins (see Tab. 5) and increases the contribution of small dust particles into the ~~AOD.~~ dust AOD. The rationale is that dust size distribution is a smoother function of logarithm of radius than radius itself, therefore interpolation is more accurate in logarithms than in radii.

To estimate the effect of these two ~~described~~ corrections, we ~~ran~~ develop the WRF-Chem simulation ~~named~~ *NON_LOG_046*, where only these two inconsistencies ~~had not been~~ are not fixed, and ~~compared~~ compare the resulting AOD with that from the *ALL_OK* run. ~~AOD values were~~ The AOD values are computed as described in Appendix C. ~~The effect is as expected, i.e., the AOD increased~~ As expected, the AOD increases after the corrections~~were made; see~~ . Fig. 3 ~~showing the comparison of the~~ compares the AOD obtained from two (with and without corrections) WRF-Chem runs with AERONET AOD at *KAUST Campus*, *Mezaira* and *Sede Boker*. Because AERONET conducts measurements during daylight hours only, we ~~interpolated~~ interpolate WRF-Chem AOD's to the AERONET measurement times.

To quantify the capability of the WRF-Chem ~~to reproduce~~ in reproducing the AERONET AOD, we ~~calculated~~ calculate the Pearson correlation coefficient R and mean bias (see Appendix B) of simulated AOD with respect to the AERONET AOD

Table 5. Dust mass redistribution between GOCART and ~~MOZAIC~~ MOSAIC bins based a) on the assumption that bin concentration is a function of radius, and b) on the assumption that bin concentration is a function of natural logarithm radius.

a)						
	~~MOZ_1~~ MOS_1	~~MOZ_2~~ MOS_2	~~MOZ_3~~ MOS_3	~~MOZ_4~~ MOS_4	~~MOZ_5~~ MOS_5	~~MO~~
$DUST_1$	0.0	0.0	0.062	0.174	0.347	
$DUST_2$	0.0	0.0	0.0	0.0	0.0	
$DUST_3$	0.0	0.0	0.0	0.0	0.0	
$DUST_4$	0.0	0.0	0.0	0.0	0.0	
~~$DUST_5$ 0.0 0.0 0.0 0.0 0.0 0.0 0.0 0.0~~ height	b)					
$DUST_1$	0.0	0.0	0.194	0.301	0.301	
$DUST_2$	0.0	0.0	0.0	0.0	0.0	
$DUST_3$	0.0	0.0	0.0	0.0	0.0	
$DUST_4$	0.0	0.0	0.0	0.0	0.0	
~~$DUST_5$ 0.0 0.0 0.0 0.0 0.0 0.0 0.0 0.0~~ height						

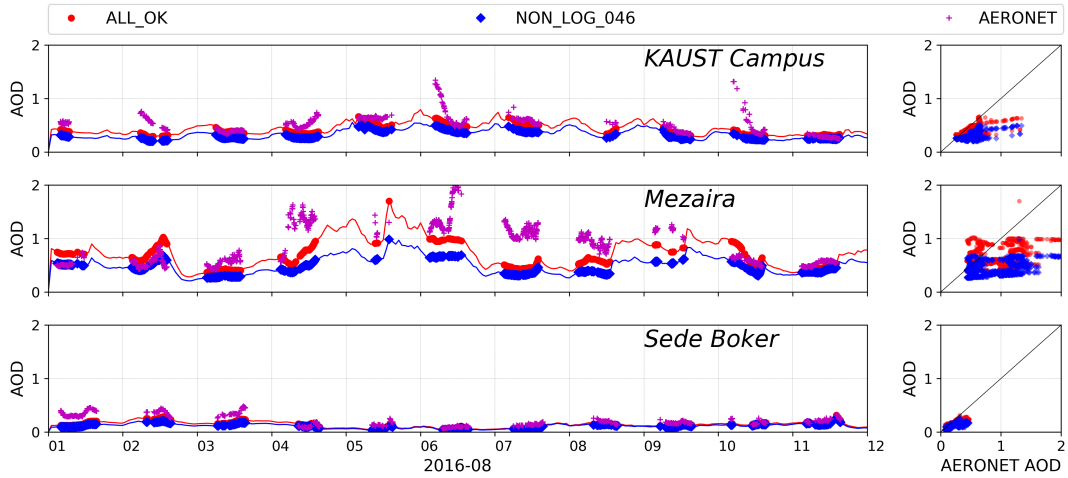

Figure 3. AOD time-series (left) and scatter plots (right) from *NON_LOG_046* and *ALL_OK* runs (blue and red lines) and AERONET AOD (purple stars) at *KAUST Campus, Mezaira, Sede Boker*. WRF-Chem's AOD is interpolated to the times (blue diamonds and red dots) when AERONET AOD measurements were conducted.

observations for the entire simulation period (see Tab. 6). The ~~changes improved the correlation coefficient R~~ corrections improve the correlation for *Mezaira* and *Sede Boker* and ~~there was~~ cause a twofold reduction in the mean bias in *KAUST Campus* and *Mezaira*. ~~In both runs, the~~ The magnitude and temporal evolution of the AOD time-series ~~are well correlated with~~ is well correlated in both runs (with and without corrections) with the observed AERONET AOD at all sites only ~~in the absence of dust events or~~ when the AERONET AOD ~~is below~~ < 1. ~~In other cases~~For dusty conditions with AOD > 1,

Table 6. Pearson correlation coefficient *R* and mean bias calculated for AOD time-series from two runs with respect to AERONET AOD observations.

	KAUST Campus		*Mezaira*		*Sede Boker*	
	R	bias	*R*	bias	*R*	bias
ALL_OK	0.66	-0.10	0.42	-0.19	0.75	-0.07
NON_LOG_046	0.66	-0.20	0.36	-0.38	0.67	-0.11

WRF-Chem with the original ~~GOCART-WRF~~ GOCART scheme (*dust_opt*=1) struggles to capture ~~strong dust storms when AERONET AOD is higher than 1. We found~~ the observations. We find the worst correlation (R=0.42) and highest mean bias (-0.19) with AERONET AOD at the *Mezaira* station, which is located in a major dust source region (see Fig. 1). We ~~obtained~~ obtain higher correlations with AERONET AOD of 0.66 and 0.75 for *KAUST Campus* and *Sede Boker* stations, respectively~~,~~ ~~both of which~~ . Both of these stations are located outside the main dust source regions.

Figure 4 shows the averaged AOD ~~time-series and scatter plots~~ fields obtained from the *ALL_OK* and *NON_LOG_046* runs, as well as their relative bias (%). ~~On average,~~ We conclude that due to these two inconsistencies, ~~AOD was~~ dust AOD in the original WRF-Chem v3.2 is underestimated by 25-30% over the ME. Over Libya, Egypt, Oman, Iran, Azerbaijan, Turkmenistan, and Pakistan, ~~this difference reached~~ the difference is even higher, reaching 30-35%.

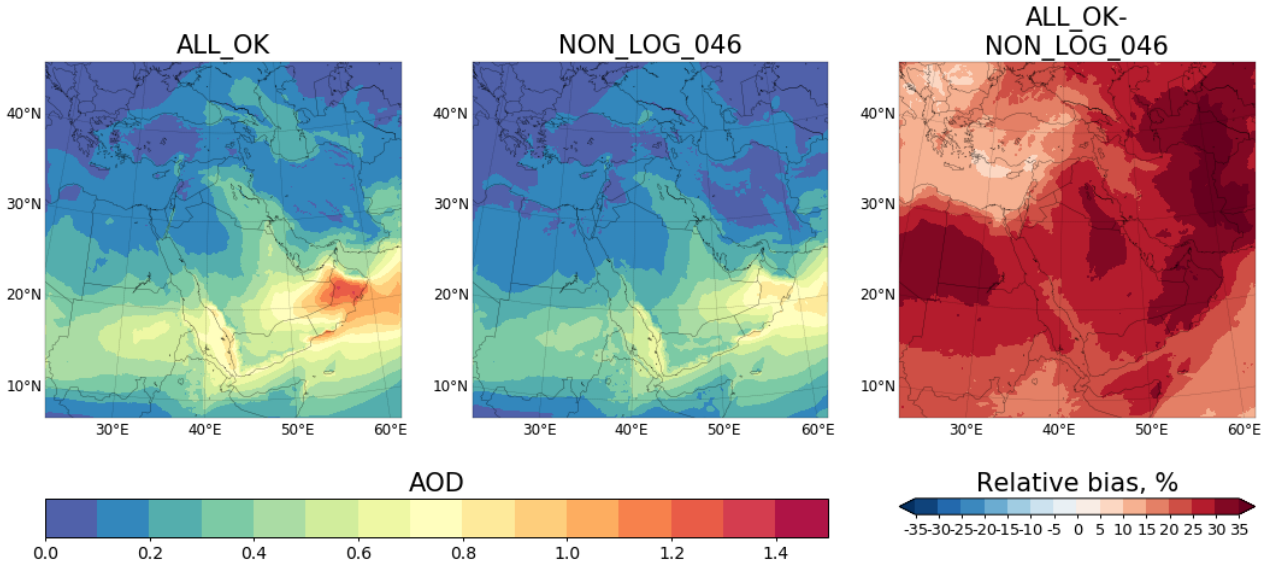

Figure 4. Averaged AOD fields obtained from *ALL_OK* and *NON_LOG_046* runs and their relative bias (%).

3.3 ~~Dust and sea salt gravitational settling~~Gravitational Settling

We ~~found that the~~ find that in the original WRF-Chem code the gravitational settling of dust and sea salt ~~was~~ is calculated incorrectly. ~~Instead of transport the dust and sea salt mass between the layers, the~~ The default finite-difference scheme ~~transported their mass mixing ratios not taking into account the dry air density variation with the height~~(implemented in the subroutine *settling()* file *module_gocart_settling.F*) does not account for change in air density when it calculates deposition mass flux. Thus, in the course of the gravitational settling the total mass of dust and sea salt in the atmosphere ~~was increasing and this, eventually, led to the violation of their mass balance. We therefore modified the default~~ increases, violating their mass balances. We introduce the new finite-difference scheme, which ~~allowed to conserve the~~ allows conservation of the mass of dust and sea salt ~~total mass in~~ in the course of gravitational settling ~~, see Appendix ??. This~~ in the atmosphere. The new finite-difference scheme is ~~implemented in the subroutine *settling()* file *module_gocart_settling.F*.~~ provided below.

The change of aerosol mixing ratio due to gravitational settling at downward directed velocity w is given by the following differential equation:

$$\frac{\partial(\rho\, q)}{\partial t} = \frac{\partial(\rho\, q\, w)}{\partial z}, \tag{3}$$

where q is the aerosol mass mixing ratio ($\mu g/kg$) and ρ is the dry air density (kg/m^3). Using the first-order upwind scheme, this equation can be discretized into the following form:

$$\frac{q_k^{n+1}\,\rho_k^{n+1} - q_k^n\,\rho_k^n}{\Delta t} = \frac{q_{k+1}^n\,\rho_{k+1}^{n+1}\,w_{k+1}^n - q_k^n\,\rho_k^{n+1}\,w_k^n}{\Delta z_k}, \tag{4}$$

where Δz_k is the depth of the k model level, Δt is the model time step. Subscript k denotes the model levels and superscript n is the time-level. Taking into account that the calculation of gravitational settling is split from the calculation of the continuity equation, we assume $\rho_k^{n+1} \approx \rho_k^n$ and get the following solution:

$$q_k^{n+1} = q_k^n\left(1 - \frac{\Delta t\, w_k^n}{\Delta z_k}\right) + q_{k+1}^n\,\frac{\Delta t\, w_{k+1}^n}{\Delta z_k}\,\frac{\rho_{k+1}^{n+1}}{\rho_k^{n+1}}. \tag{5}$$

Equation 5 is solved for each model column from the top to the bottom.

To validate the modified finite-difference scheme, we ~~zeroed~~ zero dust emissions across the whole domain, except for the ~~200x200~~ 200 km×200 km area located at the center of the domain; see Fig. 1. ~~Dust emissions within this area were allowed only within~~ Only the first 10 simulation hours ~~. We prohibited~~ of dust emissions within this area are included. We prohibit the inflow of dust from the domain boundaries by zeroing the corresponding boundary conditions~~and we zeroed~~ , and we zero the initial dust concentrations to simplify ~~the~~ calculation of the dust mass balance, which we ~~computed~~ compute using the following balance relation:

$$Dust\ in\ the\ atmosphere\ = Emitted\ dust - (Grav.\ settled\ dust + Dry\ deposited\ dust) \tag{6}$$

The amount of dust in the atmosphere is controlled by ~~the~~ dust emission and dust deposition~~, which includes~~ . The latter comprises gravitational settling and dry deposition. For the sake of clarity, we refrain from introducing other dust removal pro-

cesses, such as ~~resolved wet deposition (*wetscav_onoff=0*) and~~ sub-grid wet deposition (*conv_tr_wetscav=0*). The procedure of calculation of these diagnostics using the WRF-Chem output is provided in Appendix F.

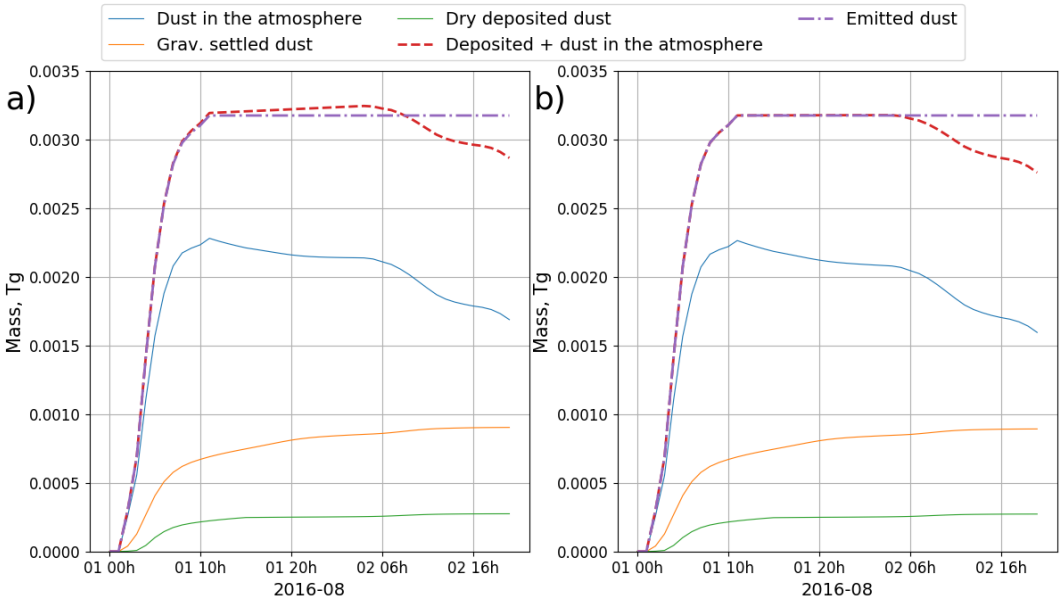

Figure 5. Dust mass balance check: a) before and b) after correction of ~~the~~ gravitational settling. $Deposited\ dust = Grav.\ settled\ dust + Dry\ deposited\ dust$.

Figure 5 demonstrates the evolution of the components of the dust mass balance ~~obtained~~ (see eq. 6) from the two runs, ~~which were performed before and after the~~ with and without correction of the gravitational settling procedure. For the analysis, we took only the first 40 hours of output because, after that time ~~, a significant amount of dust will have already left the domain through the lateral boundaries~~ the dust plume reaches the lateral boundaries of the domain. As shown in Fig. 5a, the red dashed line ~~, which corresponds~~ corresponding to the sum of deposited mass and dust mass in the atmosphere diverges from the purple dash-dotted line, which corresponds to the mass of emitted dust. This difference reaches 2.16% before the ~~emitted dust~~ dust plume reaches the boundaries of the domain. ~~This difference is caused by increasing the amount of dust in the atmosphere (blue line)~~ The run using the original gravitational settling gains the dust mass represented by the blue line, due to the error in calculating ~~the gravitational settling. A larger amount of dust in the atmosphere eventually leads to an increased amount of deposited dust (green and yellow lines).~~ gravitational settling, as discussed above. This is in contrast with Fig. 5b, where we see perfect agreement between the ~~amount~~ amounts of deposited dust plus dust in the atmosphere and ~~amount of~~ emitted dust until the dust plume reaches the boundaries of the domain. Thus, this inconsistency in the gravitational settling subroutine is significant, as the error of 2.16% of total emitted mass accumulates within ≈20 hours.

~~This effect become more~~ For larger domain this imbalance will be more significant. This effect is especially important in the ~~simulation over the~~ low-latitude desert regions. Zhang et al. (2015); Dipu et al. (2013); Huang et al. (2010) reported that

~~over the deserts, the~~ in dry subtropics the boundary layer height can reach ~~up to 6.6~~ 6-7 km, which promotes the transport of dust particles to this altitude. ~~Once lifted to this height by strong convection, dust particles can then be transported by the jet streams over long distances from the emission areas (Liu et al., 2008). When the dust particles cross more vertical layers on the way down, more error~~ When dust particles are settling from higher altitudes, a larger mass imbalance is accumulated.

We ~~estimated~~ estimate the effect of the gravitational settling error by comparing averaged total dust column loadings (see Fig. 6a), accumulated gravitationally settled dust (see Fig. 6b), and averaged dust and sea salt PM_{10} surface concentrations (see Fig. 6c) obtained in *ALL_OK* and *NOT_FIXED_GRAV_SETTLING* runs. We ~~performed the~~ perform a comparison in terms of relative ~~bias~~ differences (%) in the runs, with and without corrections. Dust column loadings, gravitationally settled dust, and PM_{10} surface concentrations ~~were~~ are calculated according to the methodology described in Appendix D, F2, E, respectively. According to Fig. 6a,b,c, we observe ~~lower~~ higher negative values of relative bias over non-dust source regions (see Fig. 1), i.e., over Sudan, Turkey, Yemen, Eritrea, Djibouti, and Ethiopia. ~~In contrast, we observe higher values of relative bias~~ By contrast, the relative differences over dust source regions, which include Egypt and the eastern ~~Arabian Peninsula. This relative bias is caused by fine dust particles.~~ part of Arabian Peninsula, are close to zero. Coarse dust particles have shorter lifetimes in the atmosphere because of their higher deposition velocities. Thus, coarse dust particles are mostly deposited in the dust source regions, which explains ~~the low~~ close to zero values of relative bias in this region. ~~On the contrary, fine~~ Fine dust particles have longer atmospheric lifetime and thus can be transported over longer distances. The discrepancies in the descriptions of the life cycle of fine dust explain larger relative errors in non-dust regions, as mentioned above.

~~The~~ Thus, we can conclude that in the original WRF-Chem v3.2 runs, the total dust column loading ~~was~~ is overestimated by 4-6% ~~on average~~ over the ME. The computed total amount of dust in the atmosphere (see Appendix F3) was 6.41 and 6.72 Tg for *ALL_OK* and *NOT_FIXED_GRAV_SETTLING* runs, respectively. Hence, the amount of dust in the atmosphere ~~was~~ is around 4.8% higher.

~~The~~ The total amount of gravitationally settled dust ~~was~~ is overestimated by 5-10% on average over the ME. The biggest difference (15-25%) ~~was~~ is observed in Sudan, Yemen, Eritrea, Djibouti, Ethiopia, and Turkey. The computed total amount of gravitationally settled dust (see Appendix F2) was 11 and 11.55 Tg for *ALL_OK* and *NOT_FIXED_GRAV_SETTLING* runs, respectively. Hence, the amount of ~~settled dust was~~ gravitationally settled dust is around 5% higher ~~.~~ in the *NOT_FIXED_GRAV_SETTLING* run. Dust and sea salt PM_{10} surface concentrations ~~were~~ (see eq. 2 and Appendix E) are overestimated by 2-4% on average over the ME. ~~However, we observe a bigger difference~~ We observe even bigger differences (6-10%) over Eritrea, Djibouti, Ethiopia, and Turkey.

3.4 Effect of ~~initial~~ Initial and ~~boundary conditions~~Boundary Conditions

We specifically ~~conducted~~ conduct a sensitivity simulation to examine the impact of boundary conditions on PM_{10} surface concentration over the ME. In this simulation boundary conditions are constructed using the developed *Merra2BC* interpolator (Ukhov and Stenchikov, 2020) (see Appendix A~~for more details~~) and we ~~zeroed~~ zero the initial concentrations of dust and sea salt. The emissions of dust and sea salt within the domain ~~were~~ are turned off (*dust_opt*=0, *seas_opt*=0). In this instance, PM_{10} concentrations are entirely determined by the inflow from the lateral boundaries. The averaged PM_{10} surface concentrations

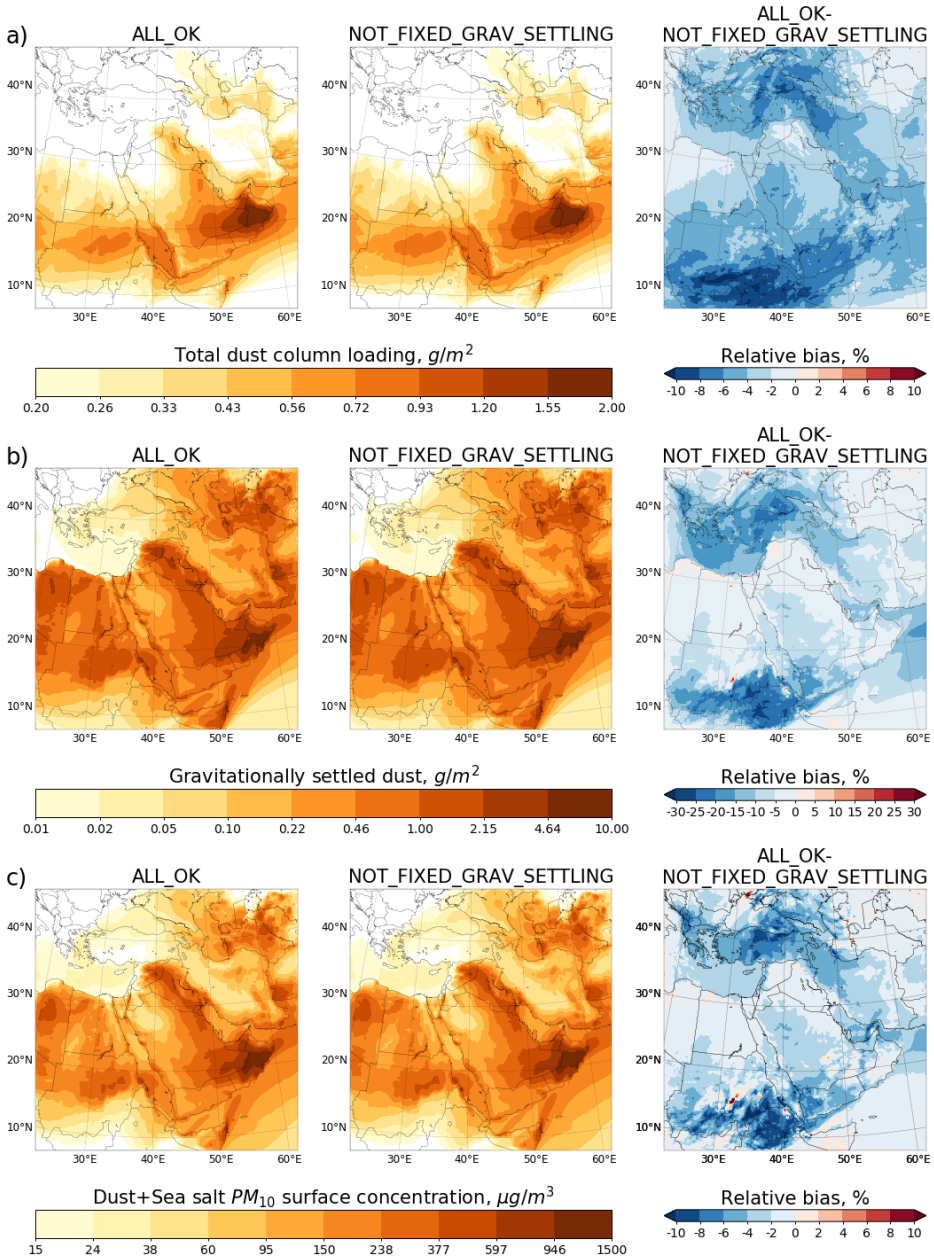

Figure 6. a) Averaged total dust column loadings ($\mathrm{g/m^2}$) and relative bias (%). b) Gravitationally settled dust ($\mathrm{g/m^2}$) and relative bias (%). c) Averaged dust and sea salt $\mathrm{PM_{10}}$ surface concentrations ($\mu\mathrm{g/m^3}$) and relative bias (%).

are presented in Fig. 7. $\mathrm{PM_{10}}$ concentrations ~~were~~ are calculated using Eq. 2. Figure 7 shows the inflow of $\mathrm{PM_{10}}$ from Africa, Central Asia and from the Indian ocean. Dust is the major contributor to the $\mathrm{PM_{10}}$ transported from Africa and Central Asia, whereas sea salt contributes to $\mathrm{PM_{10}}$ transported over the Indian ocean.

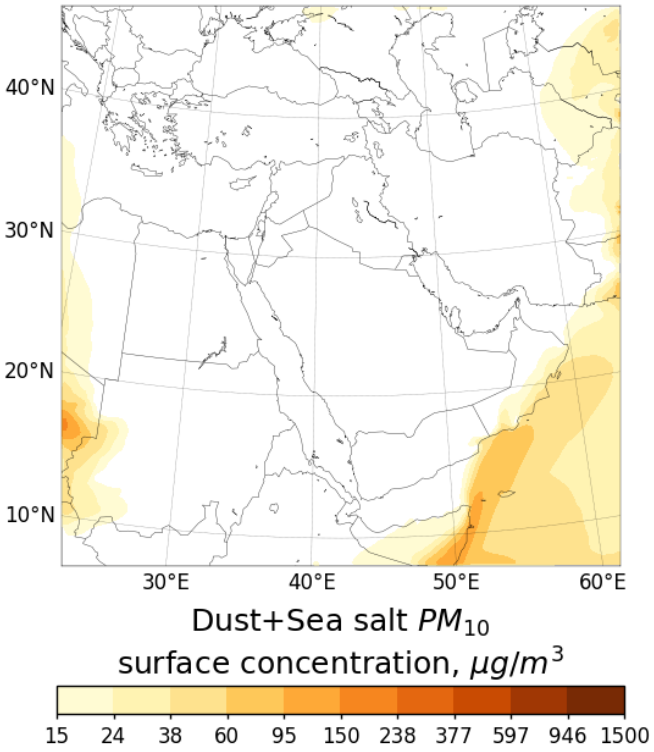

Figure 7. Effect of trans-boundary transport. Averaged dust and sea salt PM_{10} surface concentrations ($\mu g/m^3$) obtained from WRF-Chem simulation without emission of sea salt and dust.

4 Conclusions

In this paper, we discuss the inconsistencies found in the WRF-Chem v3.2 model coupled with the GOCART aerosol module~~, all of which we have~~. All of these inconsistencies are rectified in the WRF-Chem v4.1.3 code release. Here, we demonstrate the effect of the code rectification on ~~the~~ WRF-Chem model performance. We also demonstrate the methodology ~~on how~~ we employ to calculate diagnostics, which we ~~used~~ then use to estimate the ~~effect~~ effects of the changes made. To make these assessments, we ~~configured~~ configure the WRF-Chem domain over the ME and ~~ran it on~~ run it with 10 km grid resolution~~during~~. The runs under discussion in this paper were performed over the period of 1-12 August, 2016. The effect of each inconsistency was estimated using ~~individual~~ specifically designed WRF-Chem ~~run when~~ runs where only one model inconsistency was activated.

We found that in WRF-Chem v3.2 coupled with GOCART, the inconsistency in diagnostics of PM surface concentration led to a 7% underestimation of $PM_{2.5}$ and 5% overestimation of PM_{10}. Due to ~~the omission of the contribution of sub-micron dust particles in the calculation of~~ drawback in mapping of dust particles with radii between 0.1 and 0.46 µm from GOCART to MASAIC bins for Mie calculations of aerosol optical properties, the AOD was underestimated by 25-30%~~on average~~. This led

to higher dust emissions and surface PM concentrations, because the WRF-Chem model is tuned to fit the simulated AOD to AERONET observations. This ~~could explain~~ explains the inconsistencies found in Kumar et al. (2014); Eltahan et al. (2018); Flaounas et al. (2017). ~~In particular,~~ Flaounas et al. (2017) noted that ~~realistic values of AOD produced strong dust emissions and, as a result, very large~~ the model simulates realistic AODs when dust emissions are exaggerated, which in turn results in exaggerated dust surface concentrations~~and vice versa, i. e.~~. Conversely, realistic reproduction of dust concentration yields ~~too small AOD values~~AODs that are smaller than in observations. Because of the error in calculating ~~the~~ gravitational settling, dust column loadings were overestimated by 4-6% and the amount of gravitationally settled dust was overestimated by 5-10%. The contribution of dust and sea salt into PM_{10} surface concentration was overestimated by 2-4% on average over the ME.

The simultaneous effects of the different inconsistencies may amplify the total effect. For instance, AOD underestimation causes higher dust emissions (as mentioned above), which causes higher dust surface concentrations and increased production of dust in the atmosphere due to the error in gravitational settling. ~~Consequently~~As a consequence, dust surface concentrations will be ~~additionally~~ further increased. Finally, an already high PM_{10} surface concentration will be further overestimated due to the incorrect calculation of PM_{10}. Thus, the proposed improvements ~~also~~ help to explain the considerable bias towards higher PM_{10} concentrations found in ~~Ma et al. (2019); Flaounas et al. (2017); Su and Fung (2015); Nabavi et al. (2017); Rizza et al. (2017); Eltah~~ (Ma et al., 2019; Flaounas et al., 2017; Su and Fung, 2015; Nabavi et al., 2017; Rizza et al., 2017; Eltahan et al., 2018).

~~We also developed a new~~ In the course of improving the simulation of natural and anthropogenic aerosols and chemicals, we developed the capability to use MERRA-2 reanalysis for constructing WRF-Chem initial and boundary conditions for chemical species ~~, and aerosolsusing the interpolator~~ and aerosols. The interpolation utility *Merra2BC* ~~, see Appendix A~~was coded for this purpose. Boundary conditions constructed using MERRA-2 reanalysis ~~allow to~~ more realistically account for the trans-boundary transport of aerosols. *Merra2BC* is made available to the community.

~~Results of this work can be useful for the community~~ We believe the detailed quantification of the effects of the recent WRF-Chem code improvements are in line with open-source principles. The results of this work aim at better understanding of the model sensitivities to physical parameterizations. This work will add a greater understanding of model performance, and will be especially helpful for those who use the WRF-Chem model coupled with the GOCART aerosol module to carry out dust simulations over regions where dust plays an important role.

Code and data availability. The standard version of WRF-Chem is publicly available online at $https://github.com/wrf-model/WRF$. *Merra2BC* interpolator is available online at $https://github.com/saneku/Merra2BC$

Appendix A: Merra2BC interpolator

Merra2BC interpolator (Ukhov and Stenchikov, 2020) (available online at $https://github.com/saneku/Merra2BC$) creates initial and boundary conditions based on MERRA-2 reanalysis (Randles et al., 2017) for a WRF-Chem simulation by interpolating chemical species mixing ratios defined on the MERRA-2 grid to WRF-Chem grid. For the initial conditions,

interpolated values are written to each node of the WRF-Chem grid. For the boundary conditions, only boundary nodes are affected.

Merra2BC is written ~~on~~ in Python. The utility requires additional modules that need to be installed in the Python environment: NetCDF4 (netcdf4, https://github.com/Unidata/netcdf4-python) - interface to work with netCDF files and SciPy's (scipy, https://github.com/scipy/scipy) interpolation package.

The full MERRA-2 reanalysis data set including aerosol and gaseous collections is publicly available online (https://disc.gsfc.nasa.gov/daac-bin/FTPSubset2.pl). Depending on the requirements, all or one of the following aerosol and gaseous collections need to be downloaded: $inst3\_3d\_aer\_Nv$ - gaseous and aerosol mass mixing ratios, (kg/kg) and $inst3\_3d\_chm\_Nv$ - Carbon monoxide and Ozone mass mixing ratios, (kg/kg). Besides downloaded mass mixing ratios, pressure thickness $DELP$ and surface pressure PS fields also need to be downloaded. Spatial coverage of the MERRA-2 files should include the area of the simulation domain. The time span of the downloaded files should match with the start and duration of the simulation. More information regarding MERRA-2 files specification is provided in Bosilovich et al. (2016).

A1 Reconstruction of the pressure in MERRA-2 and in WRF-Chem

~~The atmospheric~~ Atmospheric pressure is used as a vertical coordinate. Latitude and longitude serve as the horizontal coordinates.

The MERRA-2 vertical grid has 72 model layers which are on a terrain-following hybrid $\sigma - p$ coordinate. The pressure at the model top is a fixed constant, P_{TOP}=0.01 hPa. Pressures at the model edges are computed by summing the $DELP$ starting at P_{TOP}. A representative pressure for the layer can then be obtained by averaging pressure values on adjacent edges. Indexing for the vertical coordinate is from top to bottom, i.e., the first layer is the top layer of the atmosphere (P_{TOP}), while the 72nd layer is adjacent to the earth's surface. ~~Surface pressure is set to P_{SRFC}=1000~~

In WRF-Chem, the pressure field is not given in $wrfinput\_d01$ and $wrfbdy\_d01$ files. Hence, the pressure field must be restored using surface pressure P_{SFC} taken from $met\_em\_...*$ files created by $metgrid.exe$ during the preprocessing stage. Pressure at the top of the model wrf_p_top and η-values on half levels (znu) are taken from the $wrfinput\_d01$ file. The procedure of reconstructing the pressure from $met\_em\_...*$ files using the python code is demonstrated in Fig. A1:

A2 Mapping chemical species between MERRA-2 and WRF-Chem

Merra2BC file $config.py$ contains multiplication factors to convert MERRA-2 mass mixing ratios of gases given in kg/kg into ppmv. Aerosols are converted from kg/kg to ug/kg. ~~In the case when using~~ When using the GOCART aerosol module in WRF-Chem simulation, all MERRA-2 aerosols and gases are matched with those from WRF-Chem. We ~~only need to~~ simply multiply by a factor of 10^9 to convert MERRA-2 aerosols mixing ratios given in kg/kg into ug/kg. In the case of gases, we need to multiply MERRA-2 mass mixing ratios by a ratio of molar masses M_{air}/M_{gas} multiplied by 10^6 to convert kg/kg into ppmv, where M_{gas} and M_{air} are molar masses (g/mol) of the required gas and air (28.97 g/mol), respectively. If another aerosol module is chosen in WRF-Chem, then different multiplication factors should be used.

```
def get_pressure_from_metfile(metfile):
      PSFC=metfile.variables['PSFC'][:]
      WRF_Pres = np.zeros([nz,ny,nx])
      for z_level in reversed(range(nz)):
            WRF_Pres[nz-1-z_level,:]=PSFC*znu[0,z_level] +
                        (1.0 - znu[0,z_level])*wrf_p_top
      return WRF_Pres
```

Figure A1. A python script, which reconstructs the pressure using the $met\_em\_...*$ files. nx, ny, nz - number of grid nodes in WRF-Chem domain.

A3 Interpolation procedure

A brief description of the interpolation procedure applied to the initial conditions is presented in Fig. A2.

For boundary conditions the procedure is similar, except that additional updates of ~~the domain boundaries~~ domain boundary tendencies are required and interpolation is performed for each step, where boundary conditions are applied.

A4 Typical workflow

Here are the steps describing how to work with *Merra2BC* interpolator:

1. Run $real.exe$, which will produce initial $wrfinput\_d01$ and boundary conditions $wrfbdy\_d01$ files required by WRF-Chem simulation;
2. Download required MERRA-2 files from https://disc.gsfc.nasa.gov/daac-bin/FTPSubset2.pl;
3. Download the *Merra2BC* from https://github.com/saneku/Merra2BC;
4. Edit $config.py$ file which contains:
   (a) mapping of chemical species and aerosols between MERRA-2 and WRF-Chem;
   (b) paths to $wrfinput\_d01$, $wrfbdy\_d01$, $met\_em\_...*$ files;
   (c) path to the downloaded MERRA-2 files;
5. $real.exe$ sets default boundary and initial conditions for some chemical species. *Merra2BC* adds interpolated values to the existing values, which may cause incorrect concentration values. To avoid this, run "python $zero\_fileds.py$", which will zero the required fields;
6. Run "python $main.py$", which will do the interpolation. As a result, files $wrfinput\_d01$, $wrfbdy\_d01$ will be updated by the interpolated from MERRA-2 values;
7. Modify the WRF-Chem $namelist.input$ file at section $\&chem$: set $have\_bcs\_chem = .true.$ to activate updated boundary conditions and, if ~~it is~~ needed, $chem\_in\_opt = 1$ to activate updated initial conditions;

Algorithm 1 Interpolation procedure applied to initial conditions

1: Pressure reconstruction at each node of the MERRA-2 and WRF-Chem grids.

2: **for** each 72 vertical layers in MERRA-2 grid **do**
3: Horizontal interpolation of MERRA-2 pressure on WRF-Chem latitude, longitude nodes using bivariate spline approximation (method *RectBivariateSpline* from Scipy module).

4: **Result**: MERRA-2 pressure is calculated on 72 levels but on latitude, longitude nodes of the WRF-Chem grid.

5: **for** each chemical species mixing ratio **do**
6: **for** each 72 vertical layers in MERRA-2 grid **do**
7: Horizontal interpolation of MERRA-2 species mixing ratio on WRF-Chem latitude, longitude nodes using bivariate spline approximation (method *RectBivariateSpline* from Scipy module).

8: **Result**: MERRA-2 species mixing ratio is calculated on 72 levels but on latitude, longitude nodes of WRF-Chem grid.

9: **for** each lat, long node of the WRF-Chem grid **do**
10: Vertical linear interpolation of MERRA-2 species mixing ratio on WRF-Chem vertical coordinate (method $interp1d$ from from Scipy module).

11: **Result**: MERRA-2 species mixing ratio is interpolated at each node of WRF-Chem grid.

12: Multiplying interpolated species mixing ratio by corresponding factor to convert kg/kg into ppmv or ug/kg, depending whether it gas or aerosol.

13: Updating corresponding fields in WRF-Chem $wrfinput\_d01$ file by interpolated values.

14: **Result**: WRF-Chem grid is updated by interpolated values from MERRA-2 grid.

Figure A2. Interpolation procedure applied to initial conditions.

8. Run $wrf.exe$.

Appendix B: Statistics

The following statistical parameters were used to quantify the level of agreement between estimations and observations:

Pearson correlation coefficient (R):

$$R = \frac{\sum_{i=1}^{N}\left(F_i - \bar{F}\right)\left(O_i - \bar{O}\right)}{\sqrt{\sum_{i=1}^{N}\left(F_i - \bar{F}\right)^2 \sum_{i=1}^{N}\left(O_i - \bar{O}\right)^2}}. \quad \text{(B1)}$$

Mean bias ($BIAS$):

$$bias = \frac{1}{N}\sum_{i=1}^{N}\left(F_i - O_i\right) \tag{B2}$$

where F_i is the estimated value, O_i is the observed value, $\bar{F} = \frac{1}{N}\sum_{i=1}^{N} F_i$ and $\bar{O} = \frac{1}{N}\sum_{i=1}^{N} O_i$ their averages and N is the number of data.

Appendix C: AOD calculations

WRF-Chem does not calculate AOD at 550 nm (only at 300, 400, 600, 1000 nm variables *TAUAER1*, *TAUAER2*, *TAUAER3*, *TAUAER4*, respectively), but, instead, it outputs the extinction coefficient at 550 nm (variable *EXTCOF55*). The AOD at 550 nm (AOD_{550}) ~~is~~ for (i,j) vertical column can be calculated by summing throughout the ~~atmospheric~~ vertical column of product of multiplication of the *EXTCOF55* by the Δz:

$$AOD_{550\ i,j} = \sum_{k} EXTCOF55_{i,j,k} \cdot \Delta z_{i,j,k}, \tag{C1}$$

where $\Delta z_{i,j,k}$ is the depth (m) of the (i,j,k) cell, which can be computed using the formula:

$$\Delta z_{i,j,k} = (PH_{i,j,k} + PHB_{i,j,k})/g, \tag{C2}$$

where $PH_{i,j,k}$ is the geopotential and $PHB_{i,j,k}$ is the perturbed geopotential and g=9.81 m/s^2 is the gravitational acceleration. Variables PH and PHB are taken from the WRF-Chem output.

To facilitate comparison with the model output the 550 nm ~~, AERONET~~ AOD is calculated using ~~Ångström exponent according to~~ the following relation:

$$\frac{\tau_\lambda}{\tau_{\lambda_0}} = \left(\frac{\lambda}{\lambda_0}\right)^{-\alpha}, \tag{C3}$$

where α is the Ångström exponent for the 440-675 nm wavelength range provided by AERONET, τ_λ is the optical thickness at wavelength λ, and τ_{λ_0} is the optical thickness at the reference wavelength λ_0.

Appendix D: Column loadings

WRF-Chem stores dust column ~~loading~~ loadings ($\mu g/m^2$) ~~for each dust bin~~ using variables $DUSTLOAD\_1,2,3,4,5$. Column loadings for (i,j) vertical column of other aerosols or chemical species can be computed by vertically summing throughout the ~~atmospheric~~ vertical column of product of multiplication of the mass mixing ratio q ($\mu g/kg$) by the cell depth Δz (m) (see eq. C2) and dry air density (kg/m^3). WRF outputs variable ALT, which is inverse dry air density (m^3/kg):

$$Column\ loading_{i,j} = \sum_{k} q_{i,j,k} \cdot \Delta z_{i,j,k} \cdot 1/ALT_{i,j,k} \tag{D1}$$

WRF-Chem outputs gases concentrations expressed in ppmv. Conversion from ppmv into the mass mixing ratio can be calculated using the following formula:

$$Mass\ mixing\ ratio = \mathrm{ppmv} \cdot 10^{-6} \cdot M_{gas}/M_{air}, \tag{D2}$$

where M_{gas} and M_{air} are molar masses ($\mathrm{g/mol}$) of the required gas and air (28.97 $\mathrm{g/mol}$), respectively.

Appendix E: Surface concentrations

~~To calculate surface~~ Surface concentration ($\mu\mathrm{g/m^3}$) of an aerosol ~~, we need to multiply~~ at (i, j) vertical column can be computed by multiplication of the mass mixing ratio ($\mu\mathrm{g/kg}$) at the first model level (q_1) by the corresponding dry air density ($\mathrm{kg/m^3}$) at the first model level ($1/ALT_1$):

$$Surface\ concentration_{i,j} = q_{i,j,1} \cdot 1/ALT_{i,j,1} \tag{E1}$$

To obtain gas surface concentration ($\mu\mathrm{g/m^3}$), (ppmv) needs to be converted to the mass mixing ratio; see ~~Eq~~eq. D2.

Appendix F: ~~Grid column area~~Dust mass balance

In the WRF-Chem's GOCART aerosol module, dust emissions along with three types of removal processes (dry deposition, gravitational settling, and wet scavenging) are implemented. Here, for the sake of clarity, we refrain from consideration of wet scavenging. To calculate the dust mass balance, assuming there is no flow of dust through the domain boundaries, we need to calculate the amount of dust emitted from the domain area, the amount of dust that was deposited by gravitational settling and dry deposition, and the amount of dust in the atmosphere. By default, WRF-Chem stores instantaneous values of dust emission and deposition fluxes. We modified the WRF-Chem code to accumulate the dust emission and deposition fluxes.

F1 Grid column area

In WRF, one of the following four projections can be used: the Lambert conformal, polar stereographic, Mercator, and latitude-longitude projections. These projections are implemented using map factors.

In the computational space, the grid lengths Δx (m) and Δy (m) (dx and dy variables in *namelist.input*) in x and y directions are constants. In the physical space, distances between grid points vary with position on the grid. Map factors $mx_{i,j}$ and $my_{i,j}$ for both the x and y components are used for the transformation from computational to physical space, and computed by *geogrid.exe* during the preprocessing stage. $mx_{i,j}$ and $my_{i,j}$ are defined as the ratio of the distance in computational space to the corresponding distance on the earth's surface (Skamarock et al., 2008):

$$(mx_{i,j}, my_{i,j}) = (\Delta x, \Delta y)/(distance\ on\ the\ earth_{i,j}) \tag{F1}$$

Map factors $mx_{i,j}$ and $my_{i,j}$ for each (i,j) vertical column are stored in $wrfinput\_d01$ file in variables $MAPFAC\_MX$ and $MAPFAC\_MY$, respectively. Thus, the area of (i,j) column $S_{i,j}$ (m^2) in physical space is calculated using formula:

$$S_{i,j} = (\Delta x / mx_{i,j}) \cdot (\Delta y / my_{i,j}) \tag{F2}$$

Appendix G: ~~Dust mass balance~~

~~In the WRF-Chem's GOCART aerosol module, dust emissions along with two types of removal processes (dry deposition and gravitational settling) are implemented. Wet deposition is not considered in the WRF-Chem's GOCART aerosol module.~~

~~To calculate the dust mass balance, assuming there is no flow of dust through the domain boundaries, we need to calculate the amount of dust emitted from the domain area, the amount of dust that was deposited by gravitational settling and dry deposition, and the amount of dust in the atmosphere. By default, WRF-Chem stores instantaneous values of the dust emission and deposition fluxes. We modified the WRF-Chem code to accumulate the dust emission and deposition fluxes.~~

F1 Dust emission

For demonstration purposes, we use the original GOCART-WRF dust emission scheme (*dust_opt*=1) implemented in subroutine *gocart_dust_driver()* file *module_gocart_dust.F*. In this scheme, instantaneous dust emission flux ($\mathrm{kg/s\ cell}$), calculated for each dust bin ~~,~~is stored in the variables *EDUST1,2,3,4,5*. Other dust emission schemes (*dust_opt*=2,3) store instantaneous dust emission flux expressed in ($\mathrm{g/m^2 s}$) and ($\mu\mathrm{g/m^2 s}$), respectively. Thus, multiplying this flux by Δt on each timestep and by adding the ~~obtained value~~ value obtained to the previous value, we accumulate dust emission ($\mathrm{kg/\ cell}$) from each surface grid cell. Thus, emission of ~~the~~ dust from the first dust bin $Emitted\ dust_1$ (kg) is calculated using the following formula:

$$Emitted\ dust_1 = \sum_{i,j} (S_{i,j} / \Delta x \cdot \Delta y) \cdot EDUST1_{i,j}, \tag{F1}$$

where $S_{i,j}$ is the area of the (i,j) column (m^2); see eq. F2. Here we divide $S_{i,j}$ by $\Delta x \cdot \Delta y$ to account for the fact that in the subroutine *gocart_dust_driver()* dust emission ~~were~~ are calculated in the computational space where grid cells have dimensions Δx and Δy.

F2 Gravitational settling and dry deposition

The subroutines *settling()* implemented in *module_gocart_settling.F* and *gocart_drydep_driver()* implemented in *module_gocart_drydep.F* are used to calculate gravitational settling and dry deposition of dust. By default, instantaneous gravitational and dry deposition fluxes ($\mu\mathrm{g/m^2\ s}$) are stored in variables $GRASET\_1,2,3,4,5$ and $DRYDEP\_1,2,3,4,5$, respectively. Thus, multiplying these fluxes on each timestep by the timestep Δt and the scaling coefficient 10^{-9}, and by adding ~~obtained~~ the resulting value to the previous value, we obtain accumulated gravitational and dry deposition mass per unit area expressed in ($\mathrm{kg/m^2}$).

Hence, deposition of the dust from the first dust bin due to gravitational settling ($Grav.\ settled\ dust_1$, kg) and ~~due to~~ dry deposition ($Dry.\ deposited\ dust_1$, kg) is calculated using the following formulas:

$$Grav.\ settled\ dust_1 = \sum_{i,j} S_{i,j} \cdot GRASET\_1_{i,j}, \tag{F2}$$

$$Dry.\ deposited\ dust_1 = \sum_{i,j} S_{i,j} \cdot DRYDEP\_1_{i,j}, \tag{F3}$$

where $S_{i,j}$ is the area of the (i,j) column (m^2); see eq. F2.

F3 Dust in the atmosphere

There are two approaches to calculate the amount of dust in the atmosphere ($Dust\ in\ the\ atmosphere$, kg). In the first approach we use dust column loadings (variables *DUSTLOAD_1,2,3,4,5*, $\mu\mathrm{g}/\mathrm{m}^2$). Thus, the mass of dust in the first dust bin is given:

$$Dust\ in\ the\ atmosphere_1 = 10^{-9} \cdot \sum_{i,j} S_{i,j} \cdot DUSTLOAD\_1_{i,j}\ , \tag{F4}$$

where $S_{i,j}$ is the area of the (i,j) column (m^2); see eq. F2.

In the second approach we calculate the mass of air in each grid cell, multiply it by the dust mass mixing ratio (for example $DUST_1$, $\mu\mathrm{g}/\mathrm{kg}$), and sum over all grid cells in the domain:

$$Dust\ in\ the\ atmosphere_1 = 10^{-9} \cdot \sum_{i,j} S_{i,j} \cdot \sum_{k} DUST_1{}_{i,j,k} \cdot \Delta z_{i,j,k} \cdot 1/ALT_{i,j,k}\ , \tag{F5}$$

where $\Delta z_{i,j,k}$ is the depth (m) (see eq. C2) and $ALT_{i,j,k}$ is the inverse dry air density (m^3/kg) in the grid cell (i,j,k).

Gaseous concentrations expressed in ppmv need to be converted into mass mixing ratios ($\mu\mathrm{g}/\mathrm{kg}$); see eq. D2.

Appendix G: ~~Finite-difference scheme for dust and sea salt gravitational settling~~

~~The change of aerosol mixing ratio due to the gravitational settling at directed down velocity w is given by~~

$$\frac{\partial(\rho\, q)}{\partial t} = \frac{\partial(\rho\, q\, w)}{\partial z},$$

~~where q is the aerosol mass mixing ratio () and ρ is the dry air density (). Using the first-order upwind scheme, this differential equation can be discretized into the following form:~~

$$\frac{q_k^{n+1}\ \rho_k^{n+1} - q_k^n\ \rho_k^n}{\Delta t} = \frac{q_{k+1}^n\ \rho_{k+1}^{n+1}\ w_{k+1}^n - q_k^n\ \rho_k^{n+1}\ w_k^n}{\Delta z_k},$$

where Δz_k is the depth of the k model level, Δt is the model time step. Subscript k denotes the model levels and superscript n is the time-level. Taking into account that the calculation of gravitational settling is split from calculation of the continuity equation we assume $\rho_k^{n+1} \approx \rho_k^n$ and get the following solution:

$$q_k^{n+1} = q_k^n \left(1 - \frac{\Delta t\ w_k^n}{\Delta z_k}\right) + q_{k+1}^n \frac{\Delta t\ w_{k+1}^n}{\Delta z_k} \frac{\rho_{k+1}^{n+1}}{\rho_k^{n+1}}.$$

This equation is solved for each model column from the top to the bottom.

Author contributions. A. Ukhov planned and performed the calculations, wrote the manuscript, and led the discussion. R. Ahmadov, G. Grell, and G. Stenchikov participated in the discussion and reviewed the manuscript.

Competing interests. The authors declare that they have no conflict of interest.

Acknowledgements. In this work, we used AERONET data from the *KAUST Campus* site that was maintained by Illia Shevchenko with the help of the NASA Goddard Space Flight Center AERONET team. We thank Brent Holben and Alexander Smirnov for ~~monitoring and the~~ the monitoring and regular calibrations of our instruments. We also used data from the *Sede Boker* and *Mezaira* sites and would like to thank their principal investigators Arnon Karnieli and Brent Holben.

The research reported in this publication was supported by funding from King Abdullah University of Science and Technology (KAUST). For computer time, this research used the resources of the Supercomputing Laboratory at KAUST.

Authors also would like to thank ~~the~~ two anonymous reviewers for their helpful comments.

References

Alghamdi, M. A., Almazroui, M., Shamy, M., Redal, M. A., Alkhalaf, A. K., Hussein, M. A., and Khoder, M. I.: Characterization and elemental composition of atmospheric aerosol loads during springtime dust storm in western Saudi Arabia, Aerosol Air Qual. Res, 15, 440–453, 2015.

Anisimov, A., Tao, W., Stenchikov, G., Kalenderski, S., Prakash, P. J., Yang, Z.-L., and Shi, M.: Quantifying local-scale dust emission from the Arabian Red Sea coastal plain, Atmospheric Chemistry and Physics, 17, 993–1015, 2017.

Bagnold, R.: The physics of blown sand and desert dunes: New York, William Morrow & Company, 1941.

Bangalath, H. K. and Stenchikov, G.: Role of dust direct radiative effect on the tropical rain belt over Middle East and North Africa: A high-resolution AGCM study, Journal of Geophysical Research: Atmospheres, 120, 4564–4584, https://doi.org/10.1002/2015JD023122, https://agupubs.onlinelibrary.wiley.com/doi/abs/10.1002/2015JD023122, 2015.

Banks, J. R., Brindley, H. E., Stenchikov, G., and Schepanski, K.: Satellite retrievals of dust aerosol over the Red Sea and the Persian Gulf (2005–2015), Atmospheric Chemistry and Physics, 17, 3987–4003, 2017.

Barnard, J. C., Fast, J. D., Paredes-Miranda, G., Arnott, W., and Laskin, A.: Evaluation of the WRF-Chem" Aerosol Chemical to Aerosol Optical Properties" Module using data from the MILAGRO campaign, Atmospheric Chemistry and Physics, 10, 7325–7340, 2010.

Belly, P.: Sand movement by wind, Tech. Mem. 1, US Army Coastal Eng. Res. Cent., Washington, DC, 1964.

Bian, H., Tie, X., Cao, J., Ying, Z., Han, S., Xue, Y., et al.: Analysis of a severe dust storm event over China: application of the WRF-dust model, Aerosol and Air Quality Resarch, 11, 419–428, 2011.

Bosilovich, M., Lucchesi, R., and Suarez, M.: MERRA-2: File specification GMAO Office Note No. 9 (Version 1.1), 2016.

Bukowski, J. and van den Heever, S. C.: Convective distribution of dust over the Arabian Peninsula: the impact of model resolution, Atmospheric Chemistry and Physics, 20, 2967–2986, https://doi.org/10.5194/acp-20-2967-2020, https://www.atmos-chem-phys.net/20/2967/2020/, 2020.

Cahill, B., Toumi, R., Stenchikov, G., Osipov, S., and Brindley, H.: Evaluation of thermal and dynamic impacts of summer dust aerosols on the Red Sea, Journal of Geophysical Research: Oceans, 122, 1325–1346, 2017.

Chen, S., Zhao, C., Qian, Y., Leung, L. R., Huang, J., Huang, Z., Bi, J., Zhang, W., Shi, J., Yang, L., et al.: Regional modeling of dust mass balance and radiative forcing over East Asia using WRF-Chem, Aeolian Research, 15, 15–30, 2014.

Chen, S., Yuan, T., Zhang, X., Zhang, G., Feng, T., Zhao, D., Zang, Z., Liao, S., Ma, X., Jiang, N., et al.: Dust modeling over East Asia during the summer of 2010 using the WRF-Chem model, Journal of Quantitative Spectroscopy and Radiative Transfer, 213, 1–12, 2018.

Chin, M., Ginoux, P., Kinne, S., Torres, O., Holben, B. N., Duncan, B. N., Martin, R. V., Logan, J. A., Higurashi, A., and Nakajima, T.: Tropospheric aerosol optical thickness from the GOCART model and comparisons with satellite and Sun photometer measurements, Journal of the atmospheric sciences, 59, 461–483, 2002.

Dee, D. P., Uppala, S., Simmons, A., Berrisford, P., Poli, P., Kobayashi, S., Andrae, U., Balmaseda, M., Balsamo, G., Bauer, d. P., et al.: The ERA-Interim reanalysis: Configuration and performance of the data assimilation system, Quarterly Journal of the royal meteorological society, 137, 553–597, 2011.

Dipu, S., Prabha, T. V., Pandithurai, G., Dudhia, J., Pfister, G., Rajesh, K., and Goswami, B.: Impact of elevated aerosol layer on the cloud macrophysical properties prior to monsoon onset, Atmospheric Environment, 70, 454–467, 2013.

Dubovik, O. and King, M. D.: A flexible inversion algorithm for retrieval of aerosol optical properties from Sun and sky radiance measurements, Journal of Geophysical Research: Atmospheres, 105, 20 673–20 696, 2000.

Eltahan, M., Shokr, M., and Sherif, A. O.: Simulation of severe dust events over Egypt using tuned dust schemes in weather research forecast (WRF-Chem), Atmosphere, 9, 246, 2018.

Emmons, L. K., Walters, S., Hess, P. G., Lamarque, J.-F., Pfister, G. G., Fillmore, D., Granier, C., Guenther, A., Kinnison, D., Laepple, T., et al.: Description and evaluation of the Model for Ozone and Related chemical Tracers, version 4 (MOZART-4), Geoscientific Model Development, pp. 43–67, 2010.

Engelbrecht, J. P., Stenchikov, G., Prakash, P. J., Lersch, T., Anisimov, A., and Shevchenko, I.: Physical and chemical properties of deposited airborne particulates over the Arabian Red Sea coastal plain, Atmospheric Chemistry and Physics, 17, 11 467–11 490, 2017.

Farahat, A.: Air pollution in the Arabian Peninsula (Saudi Arabia, the United Arab Emirates, Kuwait, Qatar, Bahrain, and Oman): causes, effects, and aerosol categorization, Arabian Journal of Geosciences, 9, 196, 2016.

Fast, J., Gustafson Jr, W., Easter, R., Zaveri, R., Barnard, J., Chapman, E., Grell, G., and Peckham, S.: Evolution of ozone, particulates, and aerosol direct forcing in an urban area using a new fully-coupled meteorology, chemistry, and aerosol model, J. Geophys. Res, 111, D21 305, 2006.

Fast, J., Aiken, A., Allan, J., Alexander, L., Campos, T., Canagaratna, M. R., Chapman, E., DeCarlo, P., Foy, B. d., Gaffney, J., et al.: Evaluating simulated primary anthropogenic and biomass burning organic aerosols during MILAGRO: implications for assessing treatments of secondary organic aerosols, Atmospheric Chemistry and Physics, 9, 6191–6215, 2009.

Flaounas, E., Kotroni, V., Lagouvardos, K., Klose, M., Flamant, C., and Giannaros, T. M.: Assessing atmospheric dust modelling performance of WRF-Chem over the semi-arid and arid regions around the Mediterranean, Atmos. Chem. Phys. Discuss., doi, 10, 2016.

Flaounas, E., Kotroni, V., Lagouvardos, K., Klose, M., Flamant, C., and Giannaros, T. M.: Sensitivity of the WRF-Chem (V3. 6.1) model to different dust emission parametrisation: assessment in the broader Mediterranean region, Geoscientific Model Development, 2017.

Forster, P., Ramaswamy, V., Artaxo, P., Berntsen, T., Betts, R., Fahey, D., Haywood, J., Lean, J., Lowe, D., Myhre, G., et al.: Climate change 2007: the physical science basis, Contribution of Working Group I to the Fourth Assessment Report of the Intergovernmental Panel on Climate Change, p. 212, 2007.

Fountoukis, C., Ackermann, L., Ayoub, M. A., Gladich, I., Hoehn, R. D., and Skillern, A.: Impact of atmospheric dust emission schemes on dust production and concentration over the Arabian Peninsula, Modeling Earth Systems and Environment, 2, 115, 2016.

Ghan, S. J. and Zaveri, R. A.: Parameterization of optical properties for hydrated internally mixed aerosol, Journal of Geophysical Research: Atmospheres, 112, https://doi.org/10.1029/2006JD007927, https://agupubs.onlinelibrary.wiley.com/doi/abs/10.1029/2006JD007927, 2007.

Gillette, D. A. and Passi, R.: Modeling dust emission caused by wind erosion, Journal of Geophysical Research: Atmospheres, 93, 14 233–14 242, 1988.

Ginoux, P., Chin, M., Tegen, I., Prospero, J. M., Holben, B., Dubovik, O., and Lin, S.-J.: Sources and distributions of dust aerosols simulated with the GOCART model, Journal of Geophysical Research: Atmospheres, 106, 20 255–20 273, 2001.

Gong, S.: A parameterization of sea-salt aerosol source function for sub-and super-micron particles, Global biogeochemical cycles, 17, 2003.

Grell, G. A., Peckham, S. E., Schmitz, R., McKeen, S. A., Frost, G., Skamarock, W. C., and Eder, B.: Fully coupled "online" chemistry within the WRF model, Atmospheric Environment, 39, 6957–6975, 2005.

Holben, B. N., Eck, T. F., Slutsker, I., Tanre, D., Buis, J., Setzer, A., Vermote, E., Reagan, J., Kaufman, Y., Nakajima, T., et al.: AERONET—A federated instrument network and data archive for aerosol characterization, Remote sensing of environment, 66, 1–16, 1998.

Huang, Q., Marsham, J. H., Parker, D. J., Tian, W., and Grams, C. M.: Simulations of the effects of surface heat flux anomalies on stratification, convective growth, and vertical transport within the Saharan boundary layer, Journal of Geophysical Research: Atmospheres, 115, 2010.

Jish Prakash, P., Stenchikov, G. L., Kalenderski, S., Osipov, S., and Bangalath, H. K.: The impact of dust storms on the Arabian Peninsula and the Red Sea, Atmospheric Chemistry and Physics, 2015.

Jish Prakash, P., Stenchikov, G., Tao, W., Yapici, T., Warsama, B., and Engelbrecht, J. P.: Arabian Red Sea coastal soils as potential mineral dust sources, Atmospheric Chemistry and Physics, 16, 11 991–12 004, 2016.

Kalenderski, S. and Stenchikov, G.: High-resolution regional modeling of summertime transport and impact of African dust over the Red Sea and Arabian Peninsula, Journal of Geophysical Research: Atmospheres, 121, 6435–6458, 2016.

Kalenderski, S., Stenchikov, G. L., and Zhao, C.: Modeling a typical winter-time dust event over the Arabian Peninsula and the Red Sea, Atmospheric Chemistry and Physics, 2013.

Karagulian, F., Temimi, M., Ghebreyesus, D., Weston, M., Kondapalli, N. K., Valappil, V. K., Aldababesh, A., Lyapustin, A., Chaouch, N., Al Hammadi, F., et al.: Analysis of a severe dust storm and its impact on air quality conditions using WRF-Chem modeling, satellite imagery, and ground observations, Air Quality, Atmosphere & Health, pp. 1–18, 2019.

Khan, B., Stenchikov, G., Weinzierl, B., Kalenderski, S., and Osipov, S.: Dust plume formation in the free troposphere and aerosol size distribution during the Saharan Mineral Dust Experiment in North Africa, Tellus B: Chemical and Physical Meteorology, 67, 27 170, 2015.

Kumar, R., Barth, M., Pfister, G., Naja, M., and Brasseur, G.: WRF-Chem simulations of a typical pre-monsoon dust storm in northern India: influences on aerosol optical properties and radiation budget, Atmospheric Chemistry and Physics, 14, 2431–2446, 2014.

LeGrand, S. L., Polashenski, C., Letcher, T. W., Creighton, G. A., Peckham, S. E., and Cetola, J. D.: The AFWA dust emission scheme for the GOCART aerosol model in WRF-Chem v3. 8.1, Geoscientific Model Development, 12, 131–166, 2019.

Levin, Z., Ganor, E., and Gladstein, V.: The effects of desert particles coated with sulfate on rain formation in the Eastern Mediterranean, Journal of Appl. Meteorol., 35, 1511—-1523, 1996.

Lihavainen, H., Alghamdi, M., Hyvärinen, A.-P., Hussein, T., Aaltonen, V., Abdelmaksoud, A., Al-Jeelani, H., Almazroui, M., Almehmadi, F., Al Zawad, F., et al.: Aerosols physical properties at Hada Al Sham, western Saudi Arabia, Atmospheric Environment, 135, 109–117, 2016.

Liu, S., McKeen, S., Hsie, E.-Y., Lin, X., Kelly, K., Bradshaw, J., Sandholm, S., Browell, E., Gregory, G., Sachse, G., et al.: Model study of tropospheric trace species distributions during PEM-West A, Journal of Geophysical Research: Atmospheres, 101, 2073–2085, 1996.

Liu, Z., Omar, A., Vaughan, M., Hair, J., Kittaka, C., Hu, Y., Powell, K., Trepte, C., Winker, D., Hostetler, C., et al.: CALIPSO lidar observations of the optical properties of Saharan dust: A case study of long-range transport, Journal of Geophysical Research: Atmospheres, 113, 2008.

Ma, S., Zhang, X., Gao, C., Tong, D. Q., Xiu, A., Wu, G., Cao, X., Huang, L., Zhao, H., Zhang, S., et al.: Multi-model simulations of springtime dust storms in East Asia: Implications of an evaluation of four commonly used air quality models (CMAQ v5. 2.1, CAMx v6. 50, CHIMERE v2017r4, and WRF-Chem v3. 9.1), Geoscientific Model Development, 2019.

Mani, M. and Pillai, R.: Impact of dust on solar photovoltaic (PV) performance: Research status, challenges and recommendations, Renewable and Sustainable Energy Reviews, 14, 3124 – 3131, https://doi.org/https://doi.org/10.1016/j.rser.2010.07.065, http://www.sciencedirect.com/science/article/pii/S1364032110002455, 2010.

Marticorena, B. and Bergametti, G.: Modeling the atmospheric dust cycle: 1. Design of a soil-derived dust emission scheme, Journal of Geophysical Research: Atmospheres, 100, 16 415–16 430, 1995.

Miller, R. and Tegen, I.: Climate response to soil dust aerosols, Journal of climate, 11, 3247–3267, 1998.

Munir, S., Habeebullah, T. M., Seroji, A. R., Morsy, E. A., Mohammed, A. M., Saud, W. A., Abdou, A. E., and Awad, A. H.: Modeling particulate matter concentrations in Makkah, applying a statistical modeling approach, Aerosol Air Qual. Res, 13, 901–910, 2013.

Nabavi, S. O., Haimberger, L., and Samimi, C.: Sensitivity of WRF-chem predictions to dust source function specification in West Asia, Aeolian Research, 24, 115–131, 2017.

Nguyen, H. D., Riley, M., Leys, J., and Salter, D.: Dust storm event of February 2019 in Central and East Coast of Australia and evidence of long-range transport to New Zealand and Antarctica, Atmosphere, 10, 653, 2019.

O'Neill, N., Eck, T., Smirnov, A., Holben, B., and Thulasiraman, S.: Spectral discrimination of coarse and fine mode optical depth, Journal of Geophysical Research: Atmospheres, 108, 2003.

Osipov, S. and Stenchikov, G.: Simulating the regional impact of dust on the Middle East climate and the Red Sea, Journal of Geophysical Research: Oceans, 123, 1032–1047, 2018.

Osipov, S., Stenchikov, G., Brindley, H., and Banks, J.: Diurnal cycle of the dust instantaneous direct radiative forcing over the Arabian Peninsula, Atmospheric Chemistry and Physics, 15, 9537–9553, 2015.

Parajuli, S. P., Stenchikov, G. L., Ukhov, A., and Kim, H.: Dust emission modeling using a new high-resolution dust source function in WRF-Chem with implications for air quality, Journal of Geophysical Research: Atmospheres, 124, 10 109–10 133, 2019.

Parajuli, S. P., Stenchikov, G. L., Ukhov, A., Shevchenko, I., Dubovik, O., and Lopatin, A.: Interaction of Dust Aerosols with Land/Sea Breezes over the Eastern Coast of the Red Sea from LIDAR Data and High-resolution WRF-Chem Simulations, Atmospheric Chemistry and Physics Discussions, 2020, 1–42, https://doi.org/10.5194/acp-2020-444, https://www.atmos-chem-phys-discuss.net/acp-2020-444/, 2020.

Powers, J. G., Klemp, J. B., Skamarock, W. C., Davis, C. A., Dudhia, J., Gill, D. O., Coen, J. L., Gochis, D. J., Ahmadov, R., Peckham, S. E., et al.: The weather research and forecasting model: Overview, system efforts, and future directions, Bulletin of the American Meteorological Society, 98, 1717–1737, 2017.

Prospero, J. M., Ginoux, P., Torres, O., Nicholson, S. E., and Gill, T. E.: Environmental characterization of global sources of atmospheric soil dust identified with the Nimbus 7 Total Ozone Mapping Spectrometer (TOMS) absorbing aerosol product, Reviews of geophysics, 40, 2–1, 2002.

Randles, C., da Silva, A. M., Buchard, V., Colarco, P., Darmenov, A., Govindaraju, R., Smirnov, A., Holben, B., Ferrare, R., Hair, J., et al.: The MERRA-2 aerosol reanalysis, 1980 onward. Part I: System description and data assimilation evaluation, Journal of climate, 30, 6823–6850, 2017.

Rao, A., Pillai, R., Mani, M., and Ramamurthy, P.: Influence of Dust Deposition on Photovoltaic Panel Performance, Energy Procedia, 54, 690 – 700, https://doi.org/https://doi.org/10.1016/j.egypro.2014.07.310, http://www.sciencedirect.com/science/article/pii/S1876610214011874, 4th International Conference on Advances in Energy Research (ICAER 2013), 2014.

Rizza, U., Barnaba, F., Miglietta, M. M., Mangia, C., Di Liberto, L., Dionisi, D., Costabile, F., Grasso, F., and Gobbi, G. P.: WRF-Chem model simulations of a dust outbreak over the central Mediterranean and comparison with multi-sensor desert dust observations, Atmospheric Chemistry and Physics, 17, 93, 2017.

Rizza, U., Miglietta, M. M., Mangia, C., Ielpo, P., Morichetti, M., Iachini, C., Virgili, S., and Passerini, G.: Sensitivity of WRF-Chem model to land surface schemes: Assessment in a severe dust outbreak episode in the Central Mediterranean (Apulia Region), Atmospheric Research, 201, 168–180, 2018.

Rotstayn, L. D. and Lohmann, U.: Tropical rainfall trends and the indirect aerosol effect, Journal of Climate, 15, 2103–2116, 2002.

Shao, Y.: A model for mineral dust emission, Journal of Geophysical Research: Atmospheres, 106, 20 239–20 254, 2001.

Shao, Y.: Simplification of a dust emission scheme and comparison with data, Journal of Geophysical Research: Atmospheres, 109, 2004.

Shao, Y., Ishizuka, M., Mikami, M., and Leys, J.: Parameterization of size-resolved dust emission and validation with measurements, Journal of Geophysical Research: Atmospheres, 116, 2011.

Skamarock, W. C., Klemp, J. B., Dudhia, J., Gill, D. O., Barker, D. M., Wang, W., and Powers, J. G.: A description of the advanced research WRF version 2, Tech. rep., National Center For Atmospheric Research Boulder Co Mesoscale and Microscale Meteorology Div, 2005.

Skamarock, W. C., Klemp, J. B., Dudhia, J., Gill, D. O., Barker, D., Duda, M., et al.: A description of the Advanced Research (WRF) model, Version 3, Natl. Ctr. Atmos. Res., Boulder, CO, 2008.

Sokolik, I. N. and Toon, O. B.: Direct radiative forcing by anthropogenic airborne mineral aerosols, Nature, 381, 681, 1996.

Su, L. and Fung, J. C.: Sensitivities of WRF-Chem to dust emission schemes and land surface properties in simulating dust cycles during springtime over East Asia, Journal of Geophysical Research: Atmospheres, 120, 11–215, 2015.

Sulaiman, S. A., Singh, A. K., Mokhtar, M. M. M., and Bou-Rabee, M. A.: Influence of Dirt Accumulation on Performance of PV Panels, Energy Procedia, 50, 50 – 56, https://doi.org/https://doi.org/10.1016/j.egypro.2014.06.006, http://www.sciencedirect.com/science/article/pii/S1876610214007425, technologies and Materials for Renewable Energy, Environment and Sustainability (TMREES14 – EUMISD), 2014.

Swap, R., Ulanski, S., Cobbett, M., and Garstang, M.: Temporal and spatial characteristics of Saharan dust outbreaks, Journal of Geophysical Research: Atmospheres, 101, 4205–4220, 1996.

Talbot, R., Harriss, R., Browell, E., Gregory, G., Sebacher, D., and Beck, S.: Distribution and geochemistry of aerosols in the tropical North Atlantic troposphere: Relationship to Saharan dust, Journal of Geophysical Research: Atmospheres, 91, 5173–5182, 1986.

Ukhov, A. and Stenchikov, G.: Merra2BC. Interpolation utility for boundary and initial conditions used in WRF-Chem, https://doi.org/10.5281/zenodo.3695911, 2020.

Ukhov, A., Mostamandi, S., da Silva, A., Flemming, J., Alshehri, Y., Shevchenko, I., and Stenchikov, G.: Assessment of natural and anthropogenic aerosol air pollution in the Middle East using MERRA-2, CAMS data assimilation products, and high-resolution WRF-Chem model simulations, Atmospheric Chemistry and Physics, 20, 9281–9310, https://doi.org/10.5194/acp-20-9281-2020, https://acp.copernicus.org/articles/20/9281/2020/, 2020a.

Ukhov, A., Mostamandi, S., Krotkov, N., Flemming, J., da Silva, A., Li, C., Fioletov, V., McLinden, C., Anisimov, A., Alshehri, Y. M., et al.: Study of SO Pollution in the Middle East Using MERRA-2, CAMS Data Assimilation Products, and High-Resolution WRF-Chem Simulations, Journal of Geophysical Research: Atmospheres, 125, e2019JD031 993, 2020b.

Wang, K., Zhang, Y., Yahya, K., Wu, S.-Y., and Grell, G.: Implementation and initial application of new chemistry-aerosol options in WRF/Chem for simulating secondary organic aerosols and aerosol indirect effects for regional air quality, Atmospheric Environment, 115, 716–732, 2015.

Watson, A. J., Bakker, D., Ridgwell, A., Boyd, P., and Law, C.: Effect of iron supply on Southern Ocean CO 2 uptake and implications for glacial atmospheric CO 2, Nature, 407, 730, 2000.

Yuan, T., Chen, S., Huang, J., Zhang, X., Luo, Y., Ma, X., and Zhang, G.: Sensitivity of simulating a dust storm over Central Asia to different dust schemes using the WRF-Chem model, Atmospheric Environment, 207, 16–29, 2019.

Zaveri, R. A., Easter, R. C., Fast, J. D., and Peters, L. K.: Model for simulating aerosol interactions and chemistry (MOSAIC), Journal of Geophysical Research: Atmospheres, 113, 2008.

Zender, C. S., Miller, R., and Tegen, I.: Quantifying mineral dust mass budgets: Terminology, constraints, and current estimates, Eos, Transactions American Geophysical Union, 85, 509–512, 2004.

Zhang, Y., Liu, Y., Kucera, P. A., Alharbi, B. H., Pan, L., and Ghulam, A.: Dust modeling over Saudi Arabia using WRF-Chem: March 2009 severe dust case, Atmospheric Environment, 119, 118–130, 2015.

Zhao, C., Liu, X., Leung, L., Johnson, B., McFarlane, S. A., Gustafson Jr, W., Fast, J. D., and Easter, R.: The spatial distribution of mineral dust and its shortwave radiative forcing over North Africa: modeling sensitivities to dust emissions and aerosol size treatments, Atmospheric Chemistry and Physics, 10, 8821–8838, 2010.

Zhao, C., Liu, X., Ruby Leung, L., and Hagos, S.: Radiative impact of mineral dust on monsoon precipitation variability over West Africa, Atmospheric Chemistry and Physics, 11, 1879–1893, 2011.

Zhao, C., Liu, X., and Leung, L.: Impact of the Desert dust on the summer monsoon system over Southwestern North America, Atmospheric Chemistry and Physics, 12, 3717–3731, 2012.

Zhao, C., Chen, S., Leung, L. R., Qian, Y., Kok, J., Zaveri, R., and Huang, J.: Uncertainty in modeling dust mass balance and radiative forcing from size parameterization., Atmospheric Chemistry & Physics Discussions, 13, 2013.

Zhu, X., Prospero, J., and Millero, F. J.: Diel variability of soluble Fe (II) and soluble total Fe in North African dust in the trade winds at Barbados, Journal of Geophysical Research: Atmospheres, 102, 21 297–21 305, 1997.